A Thermodynamic Model of Sulfur Distribution Ratio between $CaO–SiO_2–MgO–FeO–MnO–Al_2O_3$ Slags and Molten Steel during LF Refining Process Based on the Ion and Molecule Coexistence Theory

XUE-MIN YANG, CHENG-BIN SHI, MENG ZHANG, GUO-MING CHAI, and FEI WANG

A thermodynamic model for calculating the sulfur distribution ratio between ladle furnace (LF) refining slags and molten steel has been developed by coupling with a developed thermodynamic model for calculating the mass action concentrations of structural units in LF refining slags, *i.e.*, $CaO–SiO_2–MgO–FeO–MnO–Al_2O_3$ hexabasic slags, based on the ion and molecule coexistence theory (IMCT). The calculated mass action concentrations of structural units in $CaO–SiO_2–MgO–FeO–Al_2O_3–MnO$ slags equilibrated or reacted with molten steel show that the calculated equilibrium mole numbers or mass action concentrations of structural units or ion couples, rather than mass percentage of components, in the slags can represent their reaction abilities. The calculated total sulfur distribution ratio shows a reliable agreement with the measured or the calculated sulfur distribution ratio between the slags and molten steel by other models under the condition of choosing oxygen activity based on (FeO)–[O] equilibrium. Meanwhile, the developed thermodynamic model for calculating sulfur distribution ratio can quantitatively determine the respective contribution of free CaO, MgO, FeO, and MnO in the LF refining slags. A significant difference of desulfurization ability among free component as CaO, MgO, FeO, and MnO has been found with approximately 87–93 pct, 11.43–5.85 pct, 0.81–0.60 pct and 0.30–0.27 pct at both middle and final stages during LF refining process, respectively. A large difference of oxygen activity is found in molten steel at the slag–metal interface and in bulk molten steel. The oxygen activity in molten steel at the slag–metal interface is controlled by (FeO)–[O] equilibrium, whereas the oxygen activity in bulk molten steel is controlled by [Al]–[O] equilibrium. Decreasing the high-oxygen-activity boundary layer beneath the slag–metal interface can promote the desulfurization reaction rate effectively or shorten the refining period during the LF refining process.

DOI: 10.1007/s11663-011-9547-9

I. INTRODUCTION

THE deep desulfurization of molten steel can effectively decrease the amount of sulfide inclusions,[1–4] surface defects,[2,3] hot brittleness,[4] and hydrogen induced cracking[1,2] of the ultimate steel products. With respect to the outstanding desulfurization ability and other advantages,[5–7] such as rapid temperature adjustment, effective synthetic slag refining, easy composition adjustment, *etc.*, the ladle furnace (LF) refining process has become a conventional secondary refining technique in a combined metallurgical company to produce low- or ultralow-sulfur steels. However, solving the contradiction between refining efficiency and the refining period has attracted much attention in recent years because enhancing the LF desulfurization reaction needs longer refining time; however, improving the LF refining efficiency requires a shorter refining period.

The conditions both of thermodynamics and kinetics for desulfurization reactions during the LF refining process can be effectively promoted by ideal contact between the synthetic refining slags with high desulfurization ability[5] and molten steel by magnetic stirring as well as Ar gas stirring from the ladle bottom. As an easily obtained parameter to describe the desulfurization ability of slags at a metallurgical production spot, the sulfur distribution ratio between slags and metal has become a common parameter to describe the desulfurization ability of slags. However, only a few available sulfur distribution ratio prediction models for the LF

XUE-MIN YANG, Research Professor, is with the State Key Laboratory of Multiphase Complex Systems, Institute of Process Engineering, Chinese Academy of Sciences, Beijing 100190, P. R. China. Contact e–mail: yangxm71@home.ipe.ac.cn CHENG-BIN SHI, GUO-MING CHAI, and FEI WANG, Ph.D. Candidates and Joint-Training Students, are with the School of Metallurgical and Ecological Engineering, University of Science and Technology Beijing, Beijing 100083, P. R. China, and with Institute of Process Engineering, Chinese Academy of Sciences. MENG ZHANG, Master Degree Student and Joint-Training Student, is with the School of Metallurgical and Ecological Engineering, University of Science and Technology Beijing, and with Institute of Process Engineering, Chinese Academy of Sciences.

Manuscript submitted January 15, 2011.
Article published online August 24, 2011.

refining process have been developed according to compositions of slags as well as molten steel, although some desulfurization mathematical models[8,9] have been developed coupled with the sulfur distribution ratio prediction models and the related reaction kinetic data.

Besides the sulfur distribution ratio, the sulfide capacity proposed by Richardson and Fincham[10,11] in the 1950s has been widely used as another parameter to describe the desulfurization potential of slags. Similar to the sulfide capacity, the sulfide capacity index has been also suggested by Yang *et al.*[12] based on the sulfide capacity concept.[10,11] As the sulfide capacity has a close correlation with the sulfur distribution ratio of the same slags, some researchers have developed various sulfide capacity prediction models[13–20] from tremendous sulfide capacity data for various slags,[13–28] such as Young's model[13] and the KTH model.[14–20] Although Young's model[13] and the KTH model[14–20] have been verified for some slags,[13,14,16,17,20,26] whether Young's model[13] and KTH model[14–20] can be successfully used to predict the sulfur distribution ratio between LF refining slags and molten steel should be verified.

According to the developed thermodynamic model for calculating the sulfur distribution ratio between $CaO–SiO_2–MgO–Al_2O_3$ quaternary slags and carbon saturated hot metal[29] based on the ion and molecule coexistence theory (IMCT),[29–33] a thermodynamic model for calculating sulfur distribution ratio between $CaO–SiO_2–MgO–FeO–MnO–Al_2O_3$ hexabasic slags and molten steel, *i.e.*, the IMCT model, has been developed by coupling with a developed thermodynamic model for calculating the mass action concentrations of structural units or ion couples in the slags based on IMCT.[29–33] This model was built using compositions of the slags and molten steel sampled at initial, middle, and final stages during a 210-ton LF process of refining pipeline steel at Shougang Qian'an Iron and Steel Company Limited, Shougang Group.

The developed IMCT model for predicting the sulfur distribution ratio between LF refining slags and molten steel requires the mass action concentrations of structural units or ion couples in the slags like the developed model for predicting sulfur distribution ratio between blast furnace ironmaking slags and hot metal.[29] Under this circumstance, a thermodynamic model for calculating the mass action concentrations of structural units or ion couples in $CaO–SiO_2–MgO–FeO–MnO–Al_2O_3$ LF refining slags should be first developed. The calculated mass action concentrations of all existed structural units or ion couples in the slags, like the traditionally measured or calculated activity of components, have been also used to determine the oxygen activity of molten steel at the slag–metal interface.

The oxygen activity of both bulk molten steel and molten steel at the slag–metal interface have been calculated under the equilibrium of [Al]–[O], (Al_2O_3)–[Al], and (FeO)–[O], respectively, and compared with the measured oxygen activity by oxygen sensor at the initial, middle, and final stages during LF refining process of refining pipeline steel. The calculated mass action concentrations of ion couple $(Fe^{2+} + O^{2-})$ and simple molecule (Al_2O_3) have been used to calculate the oxygen activity of molten steel at the slag–metal interface. The developed IMCT model for calculating the sulfur distribution ratio between $CaO–SiO_2–MgO–FeO–MnO–Al_2O_3$ slags and molten steel can be used not only to calculate the total sulfur distribution ratio of the LF refining slags equilibrated or reacted with molten steel but also to determine the respective sulfur distribution ratio of ion couple with desulfurization ability, such as ion couples $(Ca^{2+} + O^{2-})$, $(Mg^{2+} + O^{2-})$, $(Fe^{2+} + O^{2-})$, and $(Mn^{2+} + O^{2-})$, or free basic oxide CaO, MgO, MnO, and FeO in the slags. Meanwhile, the respective contribution of these ion couples to the total sulfur distribution ratio between the LF refining slags and molten steel can be predicted. The calculated sulfur distribution ratio between the LF refining slags and molten steel by the developed IMCT model has been compared with that predicted by Young's model[13] and the KTH model.[14–20]

The oxygen activity gradient of molten steel at the slag–metal interface and in bulk molten steel has been revealed. The influence of a high oxygen activity boundary layer beneath the slag–metal interface on the desulfurization of LF refining slags has been verified. The desulfurization reaction mechanism of the LF refining slags from molten steel has been proposed according to the obtained results. The ultimate aim of this study is to develop a universal method for predicting the sulfur distribution ratio between slags and metal for various metallurgical process; furthermore, to provide reasonable methods for enhancing the desulfurization reaction in different metallurgical processes.

II. INDUSTRIAL TESTS

The industrial tests of 21 runs were carried out in a 210-ton LF of refining pipeline steel at Shougang Qian'an Iron and Steel Company Limited, Shougang Group. The synthetic slag with specially designed compositions was prepared for the 210-ton LF to refine a type of pipeline steel. The aimed content of sulfur in molten steel was controlled less than 20×10^{-4} pct. The sulfur content in the tapping molten steel from a 210-ton top–bottom combined blown converter is ranged from 0.0050 pct to 0.0100 pct with an average sulfur content of 0.0060 pct. According to the LF refining requirements and limitations on the steelmaking production line, the basic operation procedure of the 210-ton LF refining reactor is illustrated in Figure 1 and summarized as follows: (1) Approximately 210 tons of molten steel from steelmaking converter was tapped into a 210-ton ladle, in which approximately 900 kg Fe–Al alloys, 500 kg gradually releasing deoxidants, 1500 kg lime and other alloys was first added in the 210-ton ladle for deoxidization and composition adjustment of the molten steel to the aimed steel. The added gradually releasing deoxidants were used to decrease the oxygen potential of the residual slags from the steelmaking converter into the ladle, whereas the added Fe–Al alloy with an Al content of 40 pct was assigned to deoxidize the molten steel. The total slag amount is approximately 2000 kg in the 210-ton LF. (2) The temperature and

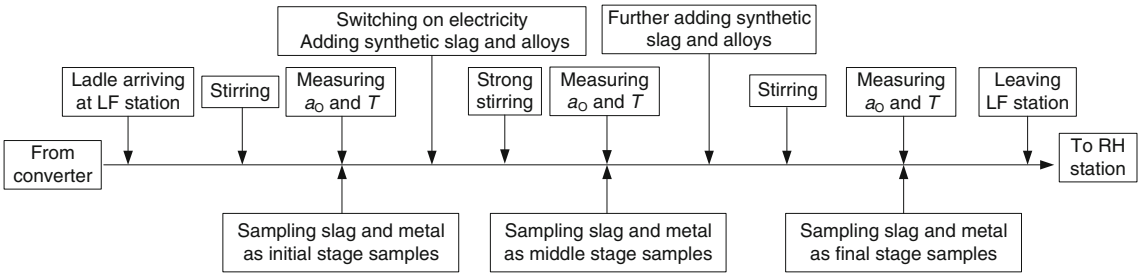

Fig. 1—Flow sheet of refining a kind of pipeline steel in a 210-ton LF.

oxygen activity of molten steel were measured immediately by a Celox low oxygen sensor simultaneously after the ladle was transported to LF refining station. The measured oxygen activity $a_{O,sensor}$ by Celox low-oxygen sensor produced by the Heraeus Electro–Nite Shanghai Company Limited (Shanghai, P. R. China) has a 3 pct deviation or a 1.5–2.0 mV deviation for the measured electromotive force (EMF). The lowest determined oxygen activity of the applied Celox low-oxygen sensor is 1.0×10^{-4}. Thereafter, Ar gas was introduced through two gas injection porous plugs from the ladle bottom to stir the molten steel for approximately 3 minutes. The diameter of the exposed molten steel for each Ar gas injection porous plug was controlled less than 100 mm. The samples of slag and molten steel were taken to analyze their chemical compositions assigned as initial stage samples. (3) A fixed amount of granulated aluminum (approximately 100 kg) was introduced into molten steel to deoxidization. Some amount of alloys with known composition and specially designed synthetic slags were introduced into the ladle. The electricity was switched on through three graphite electrodes to improve the temperature. Meanwhile, the flow rate of bottom blowing Ar gas was improved at 400–600 Nl/min to stir molten steel strongly for 12 minutes. Hereafter, samples of slags and molten steel were taken again for analyzing composition and assigned as middle stage samples. (4) Heating by electricity and stirring by bottom blowing Ar gas continues for a period, for example, of 20 minutes. The second samples of slag and molten steel at middle stage were taken again to verify whether the composition reached to the requirement of the aimed steel. If the analyzed composition of molten steel met the requirement of the aimed steel, then the samples of slag and molten steel were assigned as final stage samples. Otherwise, some amount of specially designed synthetic slags and alloy was added to adjust the composition or prolong the refining period for subsequent desulfurization. In this case, the taken samples were assigned as secondary samples at the middle stage.

Therefore, at least three samples both of slags and metal were taken to analyze the composition at each test run. The sum of the mass percentages of the components CaO, MgO, Fe_tO, Al_2O_3, MnO, and SiO_2 in each slag sample is greater than 98.5 pct. The ratio of (pct FeO) to (pct Fe_2O_3) is approximately 4:1 from the analyzed 15 slag samples. The total mass percentages of iron oxides in the LF refining slags is less than 1.0 pct; therefore, all the iron oxides in the slags were treated as FeO. The normalized compositions of slag samples at the initial, middle, and final stages during 21 test runs of the LF refining process are summarized in Tables I through III, respectively. The chemical composition, measured oxygen activity, and temperature of corresponding molten steel samples are listed in Tables I through III. Certainly, the LF refining slags have a higher binary basicity with much more Al_2O_3 content compared with blast furnace ironmaking slags.[29]

III. MODEL FOR CALCULATING MASS ACTION CONCENTRATIONS OF STRUCTURAL UNITS OR ION COUPLES IN CAO–SiO_2–MGO–FEO–MNO–Al_2O_3 SLAGS

A. *Hypotheses*

According to the classic hypotheses of IMCT described in detail elsewhere,[29–33] the main assumptions in the developed thermodynamic model for calculating the mass action concentrations of structural units or ion couple in CaO–SiO_2–MgO–FeO–MnO–Al_2O_3 LF refining slags equilibrated with molten steel can be simply summarized as follows:

(a) Structural units in the studied slags are composed of Ca^{2+}, Mg^{2+}, Fe^{2+}, Mn^{2+}, O^{2-}, and S^{2-} as simple ions, SiO_2 and Al_2O_3 as simple molecules, silicates, and aluminates and so on as complex molecules. Each structural unit has its independent position in the slags. Every cation and anion generated from the same component will take part in reactions of forming complex molecules in the form of ion couple as $(Me^{2+} + O^{2-})$.

(b) Reactions of forming complex molecules are under chemically dynamic equilibrium between the generated ion couples from simple ions and simple molecules by taking $(Ca^{2+} + O^{2-})$ and SiO_2 to form $2CaO{\cdot}SiO_2$ as an example as $2(Ca^{2+} + O^{2-}) + SiO_2 = (2CaO{\cdot}SiO_2)$.

(c) Structural units in the slags equilibrated with molten steel keep the continuity in the range of investigated concentration.

(d) Chemical reactions of forming complex molecules obey the mass action law. This implies that the chemical reaction equilibrium constant can be represented by the defined mass action concentrations in the following text.

Table I. Chemical Compositions of Slags and Molten Steel, Measured Sulfur Distribution Ratio, and Temperature at Initial Stage during a 210-ton LF Refining Process of Refining Pipeline Steel

Test No.	Chemical Composition of LF Refining Slags (mass pct)							Chemical Composition of Molten Steel (mass pct)						$a_O{}^*$ ($\times 10^{-4}$)	L_S (–)	Temperature [K (°C)]	$\sum n_i$ (mol)
	CaO	SiO_2	MgO	FeO	MnO	Al_2O_3	S	[C]	[Si]	[Mn]	[P]	[S]	$[Al]_S$				
1	49.48	7.30	9.89	0.80	0.69	31.84	0.128	0.0217	0.078	1.67	0.006	0.0046	0.0457	1.65	27.8	1824 (1551)	1.347
2	50.33	8.61	10.05	0.75	1.47	28.79	0.106	0.022	0.059	1.66	0.011	0.0038	0.0188	2.00	27.9	1836 (1563)	1.389
3	44.91	6.38	9.27	0.74	2.56	36.15	0.047	0.0245	0.076	1.65	0.008	0.0061	0.0238	2.50	7.7	1843 (1570)	1.265
4	44.63	6.11	9.50	0.70	2.50	36.57	0.049	0.027	0.082	1.61	0.008	0.0044	0.0331	2.00	11.1	1846 (1573)	1.272
5	47.32	8.97	11.15	0.86	2.00	29.71	0.078	0.0288	0.074	1.61	0.01	0.0056	0.0262	3.22	13.9	1866 (1593)	1.388
6	55.28	6.69	9.50	0.42	0.25	27.85	0.105	0.0325	0.097	1.61	0.009	0.0051	0.0307	2.00	20.6	1849 (1576)	1.484
7	48.05	6.54	10.04	0.94	0.88	33.55	0.116	0.0289	0.077	1.64	0.008	0.0043	0.0557	1.40	27.0	1834 (1561)	1.342
8	47.47	7.40	9.96	0.67	1.05	33.45	0.102	0.0238	0.053	1.66	0.009	0.0059	0.015	4.80	17.3	1844 (1571)	1.301
9	43.84	9.84	9.46	1.22	1.57	34.07	0.059	0.0272	0.09	1.67	0.009	0.0045	0.0346	4.00	13.1	1840 (1567)	1.170
10	47.33	6.33	9.73	0.71	0.67	35.24	0.103	0.0199	0.094	1.65	0.005	0.0034	0.0804	1.00	30.3	1820 (1547)	1.286
11	46.21	6.78	9.87	1.19	1.82	34.12	0.067	0.0401	0.094	1.65	0.007	0.0038	0.0287	1.00	17.6	1802 (1529)	1.316
12	45.61	7.02	9.81	1.12	1.77	34.68	0.066	0.0199	0.071	1.64	0.008	0.0039	0.0515	2.00	16.9	1839 (1566)	1.290
13	46.16	7.02	9.90	0.93	2.10	33.89	0.075	0.0221	0.083	1.64	0.005	0.0042	0.0764	2.00	17.9	1811 (1538)	1.315
14	45.96	7.15	9.96	0.99	2.40	33.54	0.068	0.0345	0.082	1.62	0.007	0.005	0.0221	2.00	13.6	1836 (1563)	1.326
15	46.27	7.17	9.95	0.99	2.22	33.41	0.070	0.0258	0.062	1.62	0.012	0.0074	0.0399	2.00	9.5	1869 (1596)	1.329
16	48.18	7.06	9.95	1.24	0.90	32.66	0.111	0.0373	0.0970	1.65	0.007	0.005	0.0246	2.00	22.2	1818 (1545)	1.342
17	48.73	6.95	9.89	0.98	0.81	32.63	0.116	0.0410	0.1060	1.72	0.008	0.0047	0.078	1.00	24.7	1844 (1571)	1.344
18	48.58	7.00	10.02	0.97	0.77	32.67	0.120	0.0411	0.0890	1.6	0.006	0.0048	0.0795	1.00	25.0	1844 (1571)	1.345
19	45.61	9.10	10.50	0.99	0.81	33.00	0.167	0.0394	0.1000	1.63	0.008	0.0054	0.028	5.00	30.9	1856 (1583)	1.262
20	46.27	8.95	10.39	1.00	0.77	32.62	0.165	0.0309	0.1050	1.65	0.006	0.0046	0.0727	1.00	35.9	1844 (1571)	1.274
21	44.74	7.66	9.74	1.13	1.15	35.57	0.164	0.0396	0.0970	1.64	0.006	0.0047	0.0326	2.00	34.9	1832 (1559)	1.236

*The oxygen activity in bulk molten steel was measured by an oxygen sensor based on a_O = [pct O]f_O rather than based on a_O = [ppmO]f_O. This note is also suitable for that in Tables II and III.

Table II. Chemical Compositions of Slags and Molten Steel, Measured Sulfur Distribution Ratio and Temperature at Middle Stage during a 210-ton LF Refining Process of Refining Pipeline Steel

Test No.	Chemical Composition of LF Refining Slags (mass pct)							Chemical Composition of Molten Steel (mass pct)						a_O^* ($\times 10^{-4}$)	L_S (–)	Temperature [K (°C)]	$\sum n_i$ (mol)
	CaO	SiO_2	MgO	FeO	MnO	Al_2O_3	S	[C]	[Si]	[Mn]	[P]	[S]	$[Al]_S$				
1	53.21	8.03	10.00	0.73	0.30	27.73	0.173	0.0350	0.146	1.80	0.007	0.0013	0.0462	3.42	133.1	1902 (1629)	1.447
2	52.63	7.99	10.03	0.68	0.42	28.25	0.166	0.0363	0.133	1.78	0.011	0.0010	0.0147	8.00	166.0	1921 (1648)	1.434
3	55.85	8.00	9.41	0.68	0.37	25.70	0.099	0.0396	0.153	1.81	0.009	0.0009	0.0384	6.00	110.0	1920 (1647)	1.494
4	50.52	5.81	10.00	0.75	0.25	32.67	0.152	0.0367	0.134	1.83	0.009	0.0017	0.0495	3.00	89.4	1882 (1609)	1.397
5	51.11	6.46	9.95	0.94	0.30	31.23	0.160	0.0414	0.142	1.82	0.011	0.0010	0.0331	6.00	160.0	1925 (1652)	1.413
6	48.87	8.22	10.80	0.84	1.41	29.87	0.088	0.0423	0.138	1.82	0.011	0.0010	0.0316	5.00	88.0	1876 (1603)	1.403
7	54.26	7.65	9.30	0.71	0.46	27.62	0.128	0.0406	0.135	1.81	0.008	0.0007	0.0262	5.30	182.9	1924 (1651)	1.444
8	49.99	6.48	10.01	0.88	0.41	32.24	0.140	0.0395	0.133	1.81	0.01	0.0009	0.0213	3.00	155.6	1895 (1622)	1.381
9	48.71	8.26	9.80	0.94	0.68	31.60	0.100	0.0453	0.17	1.84	0.01	0.0010	0.0326	2.00	100.0	1863 (1590)	1.308
10	51.59	7.19	9.87	0.84	0.42	30.08	0.103	0.0465	0.156	1.83	0.006	0.0008	0.0414	6.00	128.8	1935 (1662)	1.407
11	49.57	7.14	11.09	1.00	0.64	30.56	0.090	0.0474	0.144	1.83	0.008	0.0018	0.0539	4.00	50.0	1913 (1640)	1.441
12	49.85	6.89	10.85	0.93	0.58	30.90	0.094	0.0399	0.149	1.84	0.01	0.0009	0.0375	3.00	104.4	1882 (1609)	1.431
13	47.47	7.58	10.70	0.88	0.76	32.60	0.102	0.0497	0.153	1.83	0.006	0.0014	0.0265	3.00	72.9	1841 (1568)	1.334
14	47.56	7.78	10.81	0.90	0.78	32.18	0.099	0.0502	0.134	1.82	0.008	0.0015	0.0164	8.00	66.0	1929 (1656)	1.355
15	48.12	7.72	10.77	0.90	0.75	31.76	0.101	0.0385	0.122	1.88	0.012	0.0019	0.0278	6.00	53.2	1932 (1659)	1.368
16	53.71	7.62	9.78	1.06	0.45	27.38	0.133	0.0462	0.125	1.83	0.008	0.0019	0.043	5.00	70.0	1932 (1659)	1.475
17	53.16	7.54	9.82	1.04	0.49	27.94	0.133	0.0545	0.158	1.83	0.009	0.0011	0.0387	4.00	120.9	1907 (1634)	1.461
18	53.10	7.43	9.80	1.02	0.50	28.16	0.130	0.0543	0.138	1.85	0.007	0.0014	0.0422	2.00	92.9	1928 (1655)	1.459
19	52.69	8.09	9.62	1.38	0.46	27.77	0.162	0.0458	0.145	1.85	0.008	0.0018	0.0523	2.00	90.0	1880 (1607)	1.435
20	52.85	8.05	9.64	1.34	0.45	27.66	0.159	0.0398	0.141	1.86	0.007	0.0019	0.0502	2.00	83.7	1881 (1608)	1.441
21	59.49	6.87	9.38	0.59	0.17	23.50	0.208	0.0607	0.144	1.87	0.007	0.0010	0.0438	5.00	208.0	1910 (1637)	1.652

Table III. Chemical Compositions of Slags and Molten Steel, Measured Sulfur Distribution Ratio, and Temperature at Final Stage during a 210-ton LF Refining Process of Refining Pipeline Steel

Test No.	Chemical Composition of LF Refining Slags (mass pct)							Chemical Composition of Molten Steel (mass pct)						a_O^* ($\times 10^{-4}$)	L_S (–)	Temperature [K (°C)]	$\sum n_i$ (mol)
	CaO	SiO_2	MgO	FeO	MnO	Al_2O_3	S	[C]	[Si]	[Mn]	[P]	[S]	$[Al]_S$				
1	55.80	7.95	9.44	0.73	0.34	25.73	0.103	0.042	0.148	1.83	0.007	0.0012	0.0445	4.00	85.8	1889 (1616)	1.495
2	55.85	8.56	9.53	0.80	0.36	24.90	0.097	0.0396	0.159	1.86	0.012	0.0010	0.041	3.60	97.0	1901 (1628)	1.496
3	56.13	8.57	9.55	0.81	0.37	24.57	0.093	0.0441	0.156	1.85	0.009	0.0010	0.0503	3.00	93.0	1899 (1626)	1.508
4	50.68	5.55	9.84	0.87	0.25	32.80	0.152	0.0447	0.156	1.85	0.009	0.0016	0.0506	3.00	95.0	1896 (1623)	1.400
5	50.10	6.16	9.85	0.91	0.51	32.46	0.138	0.0432	0.15	1.84	0.011	0.0009	0.0444	3.00	153.3	1906 (1633)	1.385
6	50.45	5.88	9.79	0.86	0.36	32.66	0.145	0.0428	0.146	1.84	0.011	0.0010	0.0445	4.00	145.0	1893 (1620)	1.387
7	51.04	6.07	9.62	0.91	0.28	32.08	0.149	0.0435	0.155	1.85	0.009	0.0007	0.0493	3.00	212.9	1888 (1615)	1.390
8	50.63	5.65	9.89	0.75	0.27	32.81	0.148	0.0393	0.155	1.86	0.01	0.0008	0.0474	2.30	185.0	1892 (1619)	1.395
9	48.89	5.77	10.40	0.88	0.46	33.60	0.101	0.0449	0.177	1.84	0.01	0.0010	0.0526	4.00	101.0	1900 (1627)	1.385
10	50.24	5.43	11.29	0.76	0.25	32.03	0.110	0.0462	0.16	1.85	0.006	0.0009	0.0528	3.00	122.2	1907 (1634)	1.480
11	52.12	6.52	10.12	0.67	0.37	30.20	0.102	0.0492	0.147	1.84	0.008	0.0016	0.0516	4.00	63.8	1903 (1630)	1.441
12	59.08	6.26	9.23	0.67	0.17	24.59	0.151	0.0468	0.156	1.84	0.01	0.0009	0.0517	3.00	167.8	1895 (1622)	1.633
13	56.78	6.45	9.46	0.59	0.26	26.47	0.145	0.049	0.159	1.85	0.006	0.0014	0.0486	3.00	103.6	1900 (1627)	1.554
14	57.48	6.40	9.49	0.58	0.22	25.83	0.146	0.05	0.153	1.85	0.008	0.0014	0.0517	4.00	104.3	1899 (1626)	1.583
15	57.07	6.49	9.47	0.60	0.25	26.12	0.141	0.0416	0.144	1.86	0.012	0.0019	0.049	3.00	74.2	1903 (1630)	1.565
16	58.71	6.48	9.19	0.61	0.17	24.84	0.158	0.048	0.136	1.87	0.007	0.0012	0.0331	3.80	131.7	1886 (1613)	1.608
17	58.36	6.50	9.22	0.62	0.20	25.09	0.157	0.0557	0.168	1.86	0.009	0.0009	0.0541	4.00	174.4	1901 (1628)	1.598
18	58.37	6.56	9.21	0.66	0.20	25.01	0.157	0.0551	0.156	1.86	0.007	0.0011	0.0429	3.00	142.7	1909 (1636)	1.598
19	58.45	7.11	9.35	0.54	0.19	24.36	0.169	0.0458	0.145	1.85	0.008	0.0018	0.0523	4.00	93.9	1902 (1629)	1.596
20	57.60	7.27	9.28	0.63	0.23	24.98	0.168	0.0422	0.151	1.84	0.008	0.0020	0.0471	4.00	84.0	1907 (1634)	1.561
21	56.07	5.69	9.65	0.51	0.17	27.91	0.215	0.0577	0.162	1.86	0.008	0.0008	0.0382	4.00	268.8	1916 (1643)	1.553

(e) Considering the large difference of desulfurization ability among ion couples $(Ca^{2+}+O^{2-})$, $(Mg^{2+}+O^{2-})$, $(Fe^{2+}+O^{2-})$, and $(Mn^{2+}+O^{2-})$, the extracted sulfur in LF refining slags from molten steel is assumed only to be bonded as ion couple $(Ca^{2+}+S^{2-})$,[29] whereas the contents of the extracted sulfur in the LF refining slags bonded as ion couples $(Mg^{2+}+S^{2-})$, $(Fe^{2+}+S^{2-})$, and $(Mn^{2+}+S^{2-})$ are ignored, *i.e.*, treated as zero.[29] This assumption cannot largely affect the calculation precision of mass action concentrations of structural units or ion couple in the LF refining slags as well as the predicted sulfur distribution ratio between the slags and molten steel.

B. *Model for Calculating Mass Action Concentrations of Structural Units or Ion Couples in LF Refining Slags*

1. *Structural units in LF refining slags*

The six components in $CaO–SiO_2–MgO–FeO–Al_2O_3–MnO$ hexabasic slags are CaO, SiO_2, MgO, FeO, Al_2O_3, and MnO, whereas the extracted sulfur from molten steel gradually enters into the slags as CaS, MgS, FeS, and MnS with the proceeding of desulfurization reactions until desulfurization reactions reach equilibrium according to the classic metallurgical physicochemistry. However, the IMCT[29–33] suggests that the extracted sulfur in LF refining slags exists as S^{2-} as a structural unit and can be bonded with ions Ca^{2+}, Mg^{2+}, Fe^{2+}, and Mn^{2+} to form the ion couples $(Ca^{2+}+S^{2-})$, $(Mg^{2+}+S^{2-})$, $(Fe^{2+}+S^{2-})$, and $(Mn^{2+}+S^{2-})$ simultaneously. Hence, the LF refining slags will change from an open system of the initial LF refining slags without sulfur to a closed system of the final LF refining slags containing sulfur with the proceeding of LF refining process. The IMCT[29–33] can be applied only to a closed system. Therefore, the LF refining slags containing sulfur equilibrated or reacted with molten steel are chosen to replace the sulfur-free $CaO–SiO_2–MgO–FeO–MnO–Al_2O_3$ hexabasic slags.

However, only the total sulfur content in slags can be analyzed; no respective sulfur content, such as CaS, MgS, FeS, and MnS, can be provided from a metallurgical production *in situ* analysis as well as from a laboratory analysis. Considering the large difference of desulfurization ability between CaO and MgO revealed in a previous study,[29] the total S^{2-} in the slags is treated to exist as ion couple $(Ca^{2+}+S^{2-})$. No S^{2-} is bonded as ion couples as $(Mg^{2+}+S^{2-})$, $(Fe^{2+}+S^{2-})$, and $(Mn^{2+}+S^{2-})$ during the development of the thermodynamic model for calculating mass action concentrations of the structural units or the ion couples in $CaO–SiO_2–MgO–FeO–MnO–Al_2O_3$ slags as an assumption described in Section III–A. The sulfur content in all LF refining slags as listed in Tables I through III is less than 0.2 pct, which is much smaller than that of the other six components, *i.e.*, CaO, SiO_2, MgO, FeO, Al_2O_3, and MnO. Therefore, assuming the total S^{2-} as an ion couple $(Ca^{2+}+S^{2-})$ in Section III–A can only generate a negligible deviation on the amount of other structural units in the closed system of $CaO–SiO_2–MgO–FeO–MnO–Al_2O_3$ slags.

It can be reasonably obtained that there are six simple ions, including Ca^{2+}, Mg^{2+}, Fe^{2+}, Mn^{2+}, O^{2-} and S^{2-}, and two simple molecules, including SiO_2 and Al_2O_3, in the LF refining slags under desulfurization reaction equilibrium at metallurgical temperatures based on IMCT.[29–33] According to the reported ternary phase diagrams[34] of $CaO–Al_2O_3–SiO_2$, $CaO–Al_2O_3–MgO$, $CaO–MgO–SiO_2$, $MgO–Al_2O_3–SiO_2$, $CaO–FeO–SiO_2$, $Al_2O_3–SiO_2–MnO$, and $Al_2O_3–SiO_2–FeO$ slags at LF refining temperatures, *i.e.*, in a temperature range from 1800 K to 1935 K (1527 °C to 1662 °C), 24 kinds of complex molecules, such as $3CaO·SiO_2$, $2CaO·SiO_2$, $CaO·SiO_2$ and so on, can be formed in $CaO–SiO_2–MgO–FeO–MnO–Al_2O_3$ slags in the LF refining temperature range from 1800 K to 1935 K (1527 °C to 1662 °C) as listed in Table IV as assigned as *ci*. All simple ions, as well as simple and complex molecules in the studied slags in the LF refining temperature range are summarized in Table IV.

2. *Model for calculating mass action concentrations of structural units or ion couples in LF refining slags*

There are 10 components in $CaO–SiO_2–MgO–FeO–MnO–Al_2O_3$ slags equilibrated or reacted with molten steel as CaO, SiO_2, MgO, FeO, Al_2O_3, MnO, CaS, MgS, FeS, and MnS. Although the content of MgS, FeS, and MnS of three components in the slags is neglected, MgS, FeS, and MnS as three components cannot be ignored during the development of the thermodynamic model for calculating the mass action concentrations of structural units or ion couple in the slags. Under these circumstances, the mole number of previously mentioned 10 components in 100-g slags is assigned as $b_1 = n^0_{CaO}$, $b_2 = n^0_{SiO_2}$, $b_3 = n^0_{MgO}$, $b_4 = n^0_{FeO}$, $b_5 = n^0_{MnO}$, $b_6 = n^0_{Al_2O_3}$, $b_7 = n^0_{CaS}$, $b_8 = n^0_{MgS} = 0$, $b_9 = n^0_{FeS} = 0$, and $b_{10} = n^0_{MnS} = 0$ to represent the chemical composition of the slags.

The defined[29–33] equilibrium mole numbers n_i of all previously mentioned structural units in 100-g $CaO–SiO_2–MgO–FeO–MnO–Al_2O_3$ slags equilibrated or reacted with molten steel at metallurgical temperature are shown in Table IV. The total equilibrium mole number Σn_i of all structural units in 100-g LF refining slags equilibrated or reacted with molten steel can be expressed as follows:

$$\sum n_i = 2n_1 + n_2 + 2n_3 + 2n_4 + 2n_5 + n_6 + 2n_7 + 2n_8 + 2n_9 + 2n_{10} + n_{c1} + n_{c2} + \cdots + n_{c24} \quad \text{(mol)} \qquad [1]$$

The mass action concentration of the structural unit is defined as a ratio of the equilibrium mole number of structural unit i to the total equilibrium mole numbers of all structural units in a closed system with a fixed amount according to IMCT,[29–33] and it can be calculated by

$$N_i = \frac{n_i}{\sum n_i} \quad (-) \qquad [2]$$

Table IV. Expression of Structural Units as Ion Couples or Complex Molecules, Their Mole Numbers, and Mass Action Concentrations in 100-g $CaO–SiO_2–MgO–FeO–MnO–Al_2O_3$ Slags at LF Refining Temperature Based on IMCT

Item	Structural Units as Ion Couples or Molecules	Number of Structural Units or Ion Couples	Mole Number of Structural Unit n_i (mol)	Mass Action Concentration of Structural Unit or Ion Couple N_i (–)
Simple cation and anion (8)	$Ca^{2+}+O^{2-}$	1	$n_1 = n_{Ca^{2+},CaO} = n_{O^{2-},CaO} = n_{CaO}$	$N_1 = \frac{2n_1}{\sum n_i} = N_{CaO}$
	$Mg^{2+}+O^{2-}$	3	$n_3 = n_{Mg^{2+},MgO} = n_{O^{2-},MgO} = n_{MgO}$	$N_3 = \frac{2n_3}{\sum n_i} = N_{MgO}$
	$Fe^{2+}+O^{2-}$	4	$n_4 = n_{Fe^{2+},FeO} = n_{O^{2-},FeO} = n_{FeO}$	$N_4 = \frac{2n_4}{\sum n_i} = N_{FeO}$
	$Mn^{2+}+O^{2-}$	5	$n_5 = n_{Mn^{2+},MnO} = n_{O^{2-},MnO} = n_{MnO}$	$N_5 = \frac{2n_5}{\sum n_i} = N_{MnO}$
	$Ca^{2+}+S^{2-}$	7	$n_7 = n_{Ca^{2+},CaS} = n_{S^{2-},CaS} = n_{CaS}$	$N_7 = \frac{2n_7}{\sum n_i} = N_{CaS}$
	$Mg^{2+}+S^{2-}$	8	$n_8 = n_{Mg^{2+},MgS} = n_{S^{2-},MgS} = n_{MgS} \approx 0$	$N_8 = \frac{2n_8}{\sum n_i} = N_{MgS}$
	$Fe^{2+}+S^{2-}$	9	$n_9 = n_{Fe^{2+},FeS} = n_{S^{2-},FeS} = n_{FeS} \approx 0$	$N_9 = \frac{2n_9}{\sum n_i} = N_{FeS}$
	$Mn^{2+}+S^{2-}$	10	$n_{10} = n_{Mn^{2+},MnS} = n_{S^{2-},MnS} = n_{MnS} \approx 0$	$N_{10} = \frac{2n_{10}}{\sum n_i} = N_{MnS}$
Simple molecules (2)	SiO_2	2	$n_2 = n_{SiO_2}$	$N_2 = \frac{n_2}{\sum n_i} = N_{SiO_2}$
	Al_2O_3	6	$n_6 = n_{Al_2O_3}$	$N_6 = \frac{n_6}{\sum n_i} = N_{Al_2O_3}$
Complex molecules (24)	$3CaO·SiO_2$	c1	$n_{c1} = n_{3CaO·SiO_2}$	$N_{c1} = \frac{n_{c1}}{\sum n_i} = N_{3CaO·SiO_2}$
	$3CaO·2SiO_2$	c2	$n_{c2} = n_{3CaO·2SiO_2}$	$N_{c2} = \frac{n_{c2}}{\sum n_i} = N_{3CaO·2SiO_2}$
	$2CaO·SiO_2$	c3	$n_{c3} = n_{2CaO·SiO_2}$	$N_{c3} = \frac{n_{c3}}{\sum n_i} = N_{2CaO·SiO_2}$
	$CaO·SiO_2$	c4	$n_{c4} = n_{CaO·SiO_2}$	$N_{c4} = \frac{n_{c4}}{\sum n_i} = N_{CaO·SiO_2}$
	$3CaO·Al_2O_3$	c5	$n_{c5} = n_{3CaO·Al_2O_3}$	$N_{c5} = \frac{n_{c5}}{\sum n_i} = N_{3CaO·Al_2O_3}$
	$12CaO·7Al_2O_3$	c6	$n_{c6} = n_{12CaO·7Al_2O_3}$	$N_{c6} = \frac{n_{c6}}{\sum n_i} = N_{12CaO·7Al_2O_3}$
	$CaO·Al_2O_3$	c7	$n_{c7} = n_{CaO·Al_2O_3}$	$N_{c7} = \frac{n_{c7}}{\sum n_i} = N_{CaO·Al_2O_3}$
	$CaO·2Al_2O_3$	c8	$n_{c8} = n_{CaO·2Al_2O_3}$	$N_{c8} = \frac{n_{c8}}{\sum n_i} = N_{CaO·2Al_2O_3}$
	$CaO·6Al_2O_3$	c9	$n_{c9} = n_{CaO·6Al_2O_3}$	$N_{c9} = \frac{n_{c9}}{\sum n_i} = N_{CaO·6Al_2O_3}$
	$2MgO·SiO_2$	c10	$n_{c10} = n_{2MgO·SiO_2}$	$N_{c10} = \frac{n_{c10}}{\sum n_i} = N_{2MgO·SiO_2}$
	$MgO·SiO_2$	c11	$n_{c11} = n_{MgO·SiO_2}$	$N_{c11} = \frac{n_{c11}}{\sum n_i} = N_{MgO·SiO_2}$
	$MgO·Al_2O_3$	c12	$n_{c12} = n_{MgO·Al_2O_3}$	$N_{c12} = \frac{n_{c12}}{\sum n_i} = N_{MgO·Al_2O_3}$
	$2FeO·SiO_2$	c13	$n_{c13} = n_{2FeO·SiO_2}$	$N_{c13} = \frac{n_{c13}}{\sum n_i} = N_{2FeO·SiO_2}$
	$FeO·Al_2O_3$	c14	$n_{c14} = n_{FeO·Al_2O_3}$	$N_{c14} = \frac{n_{c14}}{\sum n_i} = N_{FeO·Al_2O_3}$
	$MnO·SiO_2$	c15	$n_{c15} = n_{MnO·SiO_2}$	$N_{c15} = \frac{n_{c15}}{\sum n_i} = N_{MnO·SiO_2}$
	$2MnO·SiO_2$	c16	$n_{c16} = n_{2MnO·SiO_2}$	$N_{c16} = \frac{n_{c16}}{\sum n_i} = N_{2MnO·SiO_2}$
	$MnO·Al_2O_3$	c17	$n_{c17} = n_{MnO·Al_2O_3}$	$N_{c17} = \frac{n_{c17}}{\sum n_i} = N_{MnO·Al_2O_3}$
	$3Al_2O_3·2SiO_2$	c18	$n_{c18} = n_{3Al_2O_3·2SiO_2}$	$N_{c18} = \frac{n_{c18}}{\sum n_i} = N_{3Al_2O_3·2SiO_2}$
	$2CaO·Al_2O_3·SiO_2$	c19	$n_{c19} = n_{2CaO·Al_2O_3·SiO_2}$	$N_{c19} = \frac{n_{c19}}{\sum n_i} = N_{2CaO·Al_2O_3·SiO_2}$
	$CaO·Al_2O_3·2SiO_2$	c20	$n_{c20} = n_{CaO·Al_2O_3·2SiO_2}$	$N_{c20} = \frac{n_{c20}}{\sum n_i} = N_{CaO·Al_2O_3·2SiO_2}$
	$CaO·MgO·SiO_2$	c21	$n_{c21} = n_{CaO·MgO·SiO_2}$	$N_{c21} = \frac{n_{c21}}{\sum n_i} = N_{CaO·MgO·SiO_2}$
	$CaO·MgO·2SiO_2$	c22	$n_{c22} = n_{CaO·MgO·2SiO_2}$	$N_{c22} = \frac{n_{c22}}{\sum n_i} = N_{CaO·MgO·2SiO_2}$
	$2CaO·MgO·2SiO_2$	c23	$n_{c23} = n_{2CaO·MgO·2SiO_2}$	$N_{c23} = \frac{n_{c23}}{\sum n_i} = N_{2CaO·MgO·2SiO_2}$
	$3CaO·MgO·2SiO_2$	c24	$n_{c24} = n_{3CaO·MgO·2SiO_2}$	$N_{c24} = \frac{n_{c24}}{\sum n_i} = N_{3CaO·MgO·2SiO_2}$

It should be emphasized that the mass action concentration N_i of all structural units in the form of simple ions, simple molecules, and complex molecules can be calculated directly from Eq. [2]; however, the mass action concentration N_{MeO} of ion couples, such as $(Me^{2+}+O^{2-})$, should be calculated by[29–33]

Table V. Chemical Reaction Formulas of Possibly Formed Complex Molecules, Their Standard Molar Gibbs Free Energy Changes, Equilibrium Constants and Mass Action Concentrations in CaO–SiO_2–MgO–FeO–MnO–Al_2O_3 Slags at Metallurgical Temperature

Reactions	$\Delta_r G^{\Theta}_{m,ci}$ (J/mol)	References	K^{Θ}_{ci} (–)	N_{ci} (–)
$3(Ca^{2+}+O^{2-})+(SiO_2)=(3CaO{\cdot}SiO_2)$	$-118826-6.694T$	35	$K^{\Theta}_{c1}=\frac{N_{c1}}{N_1^3N_2}$	$N_{c1}=K^{\Theta}_{c1}N_1^3N_2$
$3(Ca^{2+}+O^{2-})+2(SiO_2)=(3CaO{\cdot}2SiO_2)$	$-236814+9.623T$	35	$K^{\Theta}_{c2}=\frac{N_{c2}}{N_1^3N_2^2}$	$N_{c2}=K^{\Theta}_{c2}N_1^3N_2^2$
$2(Ca^{2+}+O^{2-})+(SiO_2)=(2CaO{\cdot}SiO_2)$	$-102090-24.267T$	36	$K^{\Theta}_{c3}=\frac{N_{c3}}{N_1^2N_2}$	$N_{c3}=K^{\Theta}_{c3}N_1^2N_2$
$(Ca^{2+}+O^{2-})+(SiO_2)=(CaO{\cdot}SiO_2)$	$-21757-36.819T$	36	$K^{\Theta}_{c4}=\frac{N_{c4}}{N_1N_2}$	$N_{c4}=K^{\Theta}_{c4}N_1N_2$
$3(Ca^{2+}+O^{2-})+(Al_2O_3)=(3CaO{\cdot}Al_2O_3)$	$-21757-29.288T$	36	$K^{\Theta}_{c5}=\frac{N_{c5}}{N_1^3N_6}$	$N_{c5}=K^{\Theta}_{c5}N_1^3N_6$
$12(Ca^{2+}+O^{2-})+7(Al_2O_3)=(12CaO{\cdot}7Al_2O_3)$	$617977-612.119T$	36	$K^{\Theta}_{c6}=\frac{N_{c6}}{N_1^{12}N_6^7}$	$N_{c6}=K^{\Theta}_{c6}N_1^{12}N_6^7$
$(Ca^{2+}+O^{2-})+(Al_2O_3)=(CaO{\cdot}Al_2O_3)$	$59413-59.413T$	36	$K^{\Theta}_{c7}=\frac{N_{c7}}{N_1N_6}$	$N_{c7}=K^{\Theta}_{c7}N_1N_6$
$(Ca^{2+}+O^{2-})+2(Al_2O_3)=(CaO{\cdot}2Al_2O_3)$	$-16736-25.522T$	36	$K^{\Theta}_{c8}=\frac{N_{c8}}{N_1N_6^2}$	$N_{c8}=K^{\Theta}_{c8}N_1N_6^2$
$(Ca^{2+}+O^{2-})+6(Al_2O_3)=(CaO{\cdot}6Al_2O_3)$	$-22594-31.798T$	37	$K^{\Theta}_{c9}=\frac{N_{c9}}{N_1N_6^6}$	$N_{c9}=K^{\Theta}_{c9}N_1N_6^6$
$2(Mg^{2+}+O^{2-})+(SiO_2)=(2MgO{\cdot}SiO_2)$	$-56902-3.347T$	36	$K^{\Theta}_{c10}=\frac{N_{c10}}{N_2N_3^2}$	$N_{c10}=K^{\Theta}_{c10}N_2N_3^2$
$(Mg^{2+}+O^{2-})+(SiO_2)=(MgO{\cdot}SiO_2)$	$23849-29.706T$	36	$K^{\Theta}_{c11}=\frac{N_{c11}}{N_2N_3}$	$N_{c11}=K^{\Theta}_{c11}N_2N_3$
$(Mg^{2+}+O^{2-})+(Al_2O_3)=(MgO{\cdot}Al_2O_3)$	$-18828-6.276T$	36	$K^{\Theta}_{c12}=\frac{N_{c12}}{N_3N_6}$	$N_{c12}=K^{\Theta}_{c12}N_3N_6$
$2(Fe^{2+}+O^{2-})+(SiO_2)=(2FeO{\cdot}SiO_2)$	$-9395-0.227T$	35,38,39	$K^{\Theta}_{c13}=\frac{N_{c13}}{N_2N_4^2}$	$N_{c13}=K^{\Theta}_{c13}N_2N_4^2$
$(Fe^{2+}+O^{2-})+(Al_2O_3)=(FeO{\cdot}Al_2O_3)$	$-59204+22.343T$	40	$K^{\Theta}_{c14}=\frac{N_{c14}}{N_4N_6}$	$N_{c14}=K^{\Theta}_{c14}N_4N_6$
$(Mn^{2+}+O^{2-})+(SiO_2)=(MnO{\cdot}SiO_2)$	$38911-40.041T$	35	$K^{\Theta}_{c15}=\frac{N_{c15}}{N_2N_5}$	$N_{c15}=K^{\Theta}_{c15}N_2N_5$
$2(Mn^{2+}+O^{2-})+(SiO_2)=(2MnO{\cdot}SiO_2)$	$36066-30.669T$	35	$K^{\Theta}_{c16}=\frac{N_{c16}}{N_2N_5^2}$	$N_{c16}=K^{\Theta}_{c16}N_2N_5^2$
$(Mn^{2+}+O^{2-})+(Al_2O_3)=(MnO{\cdot}Al_2O_3)$	$-45116+11.81T$	41	$K^{\Theta}_{c17}=\frac{N_{c17}}{N_5N_6}$	$N_{c17}=K^{\Theta}_{c17}N_5N_6$
$3(Al_2O_3)+2(SiO_2)=(3Al_2O_3{\cdot}2SiO_2)$	$-4354-10.467T$	36	$K^{\Theta}_{c18}=\frac{N_{c18}}{N_2^2N_6^3}$	$N_{c18}=K^{\Theta}_{c18}N_2^2N_6^3$
$2(Ca^{2+}+O^{2-})+(Al_2O_3)+(SiO_2)=(2CaO{\cdot}Al_2O_3{\cdot}SiO_2)$	$-116315-38.911T$	36	$K^{\Theta}_{c19}=\frac{N_{c19}}{N_1^2N_2N_6}$	$N_{c19}=K^{\Theta}_{c19}N_1^2N_2N_6$
$(Ca^{2+}+O^{2-})+(Al_2O_3)+2(SiO_2)=(CaO{\cdot}Al_2O_3{\cdot}2SiO_2)$	$-4184-73.638T$	36	$K^{\Theta}_{c20}=\frac{N_{c20}}{N_1N_2^2N_6}$	$N_{c20}=K^{\Theta}_{c20}N_1N_2^2N_6$
$(Ca^{2+}+O^{2-})+(Mg^{2+}+O^{2-})+(SiO_2)=(CaO{\cdot}MgO{\cdot}SiO_2)$	$-124683+3.766T$	35	$K^{\Theta}_{c21}=\frac{N_{c21}}{N_1N_2N_3}$	$N_{c21}=K^{\Theta}_{c21}N_1N_2N_3$
$(Ca^{2+}+O^{2-})+(Mg^{2+}+O^{2-})+2(SiO_2)=(CaO{\cdot}MgO{\cdot}2SiO_2)$	$-80333-51.882T$	36	$K^{\Theta}_{c22}=\frac{N_{c22}}{N_1N_3N_2^2}$	$N_{c22}=K^{\Theta}_{c22}N_1N_3N_2^2$
$2(Ca^{2+}+O^{2-})+(Mg^{2+}+O^{2-})+2(SiO_2)=(2CaO{\cdot}MgO{\cdot}2SiO_2)$	$-73638-63.597T$	36	$K^{\Theta}_{c23}=\frac{N_{c23}}{N_1^2N_2^2N_3}$	$N_{c23}=K^{\Theta}_{c23}N_1^2N_2^2N_3$
$3(Ca^{2+}+O^{2-})+(Mg^{2+}+O^{2-})+2(SiO_2)=(3CaO{\cdot}MgO{\cdot}2SiO_2)$	$-205016-31.798T$	37	$K^{\Theta}_{c24}=\frac{N_{c24}}{N_1^3N_2^2N_3}$	$N_{c24}=K^{\Theta}_{c24}N_1^3N_2^2N_3$

$$N_{MeO}=N_{Me^{2+},MeO}+N_{O^{2-},MeO}=\frac{n_{Me^{2+},MeO}+n_{O^{2-},MeO}}{\sum n_i}=\frac{2n_{MeO}}{\sum n_i}\quad(-)\qquad[3]$$

Therefore, all expressions of N_i for the formed ion couples from simple ions, simple molecules, and complex molecules in the LF refining slags are listed in Table IV.

The chemical reaction formulas of 24 kinds of possibly formed complex molecules, their standard molar Gibbs free energy changes $\Delta_r G^{\Theta}_{m,ci}$ as a function of absolute temperature T, reaction equilibrium constant K^{Θ}_{ci} and representation of mass action concentrations of all complex molecules N_{ci} expressed by K^{Θ}_{ci}, $N_1(N_{Cao})$, $N_2(N_{SiO_2})$, $N_3(N_{MgO})$, $N_4(N_{FeO})$, $N_5(N_{MnO})$, and $N_6(N_{Al_2O_3})$ based on the mass action law are summarized in Table V.

The mass conservation equations of 10 components in 100-g LF refining slags equilibrated or reacted with molten steel can be established from the definitions[29–33] of n_i and N_i of all structural units listed in Tables IV and V as follows:

$$\begin{aligned}b_1=&\left(\frac{1}{2}N_1+3N_{c1}+3N_{c2}+2N_{c3}+N_{c4}+3N_{c5}\right.\\&+12N_{c6}+N_{c7}+N_{c8}+N_{c9}+2N_{c19}+N_{c20}\\&\left.+N_{c21}+N_{c22}+2N_{c23}+3N_{c24}\right)\sum n_i\\=&\left(\frac{1}{2}N_1+3K^{\Theta}_{c1}N_1^3N_2+3K^{\Theta}_{c2}N_1^3N_2^2+2K^{\Theta}_{c3}N_1^2N_2\right.\\&+K^{\Theta}_{c4}N_1N_2+3K^{\Theta}_{c5}N_1^3N_6+12K^{\Theta}_{c6}N_1^{12}N_6^7\\&+K^{\Theta}_{c7}N_1N_6+K^{\Theta}_{c8}N_1N_6^2+K^{\Theta}_{c9}N_1N_6^6\\&+2K^{\Theta}_{c19}N_1^2N_2N_6+K^{\Theta}_{c20}N_1N_6N_2^2+K^{\Theta}_{c21}N_1N_2N_3\\&+K^{\Theta}_{c22}N_1N_3N_2^2+2K^{\Theta}_{c23}N_1^2N_3N_2^2\\&\left.+3K^{\Theta}_{c24}N_1^3N_2^2N_3\right)\sum n_i=n^0_{CaO}\quad(mol)\end{aligned}\qquad[4a]$$

$$b_2 = (N_2 + N_{c1} + 2N_{c2} + N_{c3} + N_{c4} + N_{c10} + N_{c11} + N_{c13} + N_{c15} + N_{c16} + 2N_{c18} + N_{c19} + 2N_{c20} + N_{c21} + 2N_{c22} + 2N_{c23} + 2N_{c24}) \sum n_i$$
$$= \left(N_2 + K_{c1}^{\Theta} N_1^3 N_2 + 2K_{c2}^{\Theta} N_1^3 N_2^2 + K_{c3}^{\Theta} N_1^2 N_2 + K_{c4}^{\Theta} N_1 N_2 + K_{c10}^{\Theta} N_2 N_3^2 + K_{c11}^{\Theta} N_2 N_3 + K_{c13}^{\Theta} N_2 N_4^2 + K_{c15}^{\Theta} N_2 N_5 + K_{c16}^{\Theta} N_2 N_5^2 + 2K_{c18}^{\Theta} N_2^2 N_6^3 + K_{c19}^{\Theta} N_1^2 N_2 N_6 + 2K_{c20}^{\Theta} N_1 N_2^2 N_6 + K_{c21}^{\Theta} N_1 N_2 N_3 + 2K_{c22}^{\Theta} N_1 N_2^2 N_3 + 2K_{c23}^{\Theta} N_1^2 N_2^2 N_3 + 2K_{c24}^{\Theta} N_1^3 N_2^2 N_3\right)$$
$$\sum n_i = n_{SiO_2}^0 \quad \text{(mol)} \qquad [4b]$$

$$b_3 = \left(\frac{1}{2}N_3 + 2N_{c10} + N_{c11} + N_{c12} + N_{c21} + N_{c22} + N_{c23} + N_{c24}\right) \sum n_i$$
$$= \left(\frac{1}{2}N_3 + 2K_{c10}^{\Theta} N_2 N_3^2 + K_{c11}^{\Theta} N_2 N_3 + K_{c12}^{\Theta} N_3 N_6 + K_{c21}^{\Theta} N_1 N_2 N_3 + K_{c22}^{\Theta} N_1 N_3 N_2^2 + K_{c23}^{\Theta} N_1^2 N_2^2 N_3 + K_{c24}^{\Theta} N_1^3 N_2^2 N_3\right) \sum n_i = n_{MgO}^0 \quad \text{(mol)} \qquad [4c]$$

$$b_4 = \left(\frac{1}{2}N_4 + 2N_{c13} + N_{c14}\right) \sum n_i$$
$$= \left(\frac{1}{2}N_4 + 2K_{c13}^{\Theta} N_2 N_4^2 + K_{c14}^{\Theta} N_4 N_6\right) \sum n_i$$
$$= n_{FeO}^0 \quad \text{(mol)} \qquad [4d]$$

$$b_5 = \left(\frac{1}{2}N_5 + N_{c15} + 2N_{c16} + N_{c17}\right) \sum n_i$$
$$= \left(\frac{1}{2}N_5 + K_{c15}^{\Theta} N_2 N_5 + 2K_{c16}^{\Theta} N_2 N_5^2 + K_{c17}^{\Theta} N_5 N_6\right) \sum n_i$$
$$= n_{MnO}^0 \quad \text{(mol)} \qquad [4e]$$

$$b_6 = (N_6 + N_{c5} + 7N_{c6} + N_{c7} + 2N_{c8} + 6N_{c9} + N_{c12} + N_{c14} + N_{c17} + 3N_{c18} + N_{c19} + N_{c20}) \sum n_i$$
$$= (N_6 + K_{c5}^{\Theta} N_1^3 N_6 + 7K_{c6}^{\Theta} N_1^{12} N_6^7 + K_{c7}^{\Theta} N_1 N_6 + 2K_{c8}^{\Theta} N_1 N_6^2 + 6K_{c9}^{\Theta} N_1 N_6^6 + K_{c12}^{\Theta} N_3 N_6 + K_{c14}^{\Theta} N_4 N_6 + K_{c17}^{\Theta} N_5 N_6 + 3K_{c18}^{\Theta} N_2^2 N_6^3 + K_{c19}^{\Theta} N_1^2 N_2 N_6 + K_{c20}^{\Theta} N_1 N_2^2 N_6) \sum n_i = n_{Al_2O_3}^0 \quad \text{(mol)} \qquad [4f]$$

$$b_7 = \left(\frac{1}{2}N_7\right) \sum n_i = n_{CaS}^0 \quad \text{(mol)} \qquad [4g]$$

$$b_8 = \left(\frac{1}{2}N_8\right) \sum n_i = n_{MgS}^0 \approx 0 \quad \text{(mol)} \qquad [4h]$$

$$b_9 = \left(\frac{1}{2}N_9\right) \sum n_i = n_{FeS}^0 \approx 0 \quad \text{(mol)} \qquad [4i]$$

$$b_{10} = \left(\frac{1}{2}N_{10}\right) \sum n_i = n_{MnS}^0 \approx 0 \quad \text{(mol)} \qquad [4j]$$

According to the principle that the sum of mole fraction for all structural units in a fixed amount of $CaO–SiO_2–MgO–FeO–MnO–Al_2O_3$ slags under equilibrium condition is equal to 1.0, the following equation can be obtained:

$$N_1 + N_2 + N_3 + N_4 + N_5 + N_6 + N_7 + N_8 + N_9 + N_{10} + N_{c1} + N_{c2} + \cdots + N_{c24} = N_1 + \cdots + N_{10} + K_{c1}^{\Theta} N_1^3 N_2 + K_{c2}^{\Theta} N_1^3 N_2^2 + \cdots + K_{c24}^{\Theta} N_1^3 N_2^2 N_3 = \sum N_i = 1.0 \quad (-) \qquad [5]$$

The equilibrium constant K_{ci}^{Θ} of all dynamic reactions described in Table V can be calculated as follows:

$$K_{ci}^{\Theta} = \exp\left(-\Delta_r G_{m,ci}^{\Theta}/RT\right) \quad (-) \qquad [6]$$

Therefore, the equation group of Eqs. [4] and [5] is the governing equations of the developed thermodynamic model for calculating mass action concentrations N_i of structural units or ion couples in the LF refining slags equilibrated or reacted with molten steel. Obviously, the 11 unknown parameters are N_1, N_2, N_3, N_4, N_5, N_6, N_7, $N_8 \approx 0$, $N_9 \approx 0$, $N_{10} \approx 0$, and Σn_i with 11 independent equations in the developed equation group of Eqs. [4] and [5]. The unique solution of N_i, Σn_i, and n_i can be calculated by solving the algebraic equation groups of Eqs. [4] and [5] combined with the definition of N_i in Eqs. [2] and [3]. The calculated Σn_i in 100-g LF refining slags at three stages during 21 test runs of the LF refining process is summarized in Tables I through III, respectively.

3. *Meaning of mass action concentrations of structural units or ion couples in LF refining slags*

The physical meaning of N_i is the equilibrium mole fraction of structural unit i in a closed system. The essential meaning of N_i is almost consistent with the traditionally applied activity a_i of components i in slags, in which pure solid matter is chosen as the standard state and mole fraction are selected as a concentration unit. In the past two decades, Zhang *et al.*[30–33,42–48] and other researchers[49] have proved that the calculated mass action concentrations of structural units or ion couples in various slags have good corresponding relations with the measured activities of components, such as in $MnO–SiO_2$ slags,[33,42] $FeO–Fe_2O_3–SiO_2$ slags,[33,43] $CaO–SiO_2–Al_2O_3–MgO$ slags,[33,44] $CaO–FeO–SiO_2$,[33,45] $CaO–Al_2O_3–SiO_2$,[33,46] $Na_2O–$

SiO_2,[33,47] CaO–MgO slags and NiO–MgO slags,[33,48] and CaO–MgO–SiO_2–Al_2O_3–Cr_2O_3.[49] Therefore, the formulas of the reaction equilibrium constant K_i^{Θ} and the related standard molar Gibbs free energy change $\Delta_r G_{m,i}^{\Theta}$ of the reaction for forming the structural unit i as complex molecules can be presented by N_i to replace a_i according to IMCT[29–33] as listed in Table V.

According to IMCT,[29–33] the mass action concentrations correspond to all ion couples, simple molecules, and complex molecules rather than to components in slags. However, the concept of activity is based on the components in slags according to the classically metallurgical physicochemistry. Theoretically, only 10 activity data in CaO–SiO_2–MgO–FeO–MnO–Al_2O_3 slags containing sulfur as CaO, SiO_2, MgO, FeO, Al_2O_3, MnO, CaS, MgS, FeS, and MnS can be determined from viewpoints of the traditional experimental tests and classically metallurgical thermodynamics, but 34 data of mass action concentrations can be calculated in the LF refining slags based on IMCT.[29–33] Applying the expression of the mass action concentration of the ion couple ($Me^{2+} + O^{2-}$), *i.e.*, free MeO, as N_{MeO} shown in Eq. [3] or in Tables IV and V, is just for convenience to present the reaction ability of free MeO in the slags, like the MeO activity a_{MeO}. Under this circumstance, no valuable activity data of the LF refining slags have been measured or reported; therefore, the calculated mass action concentrations N_i of the structural unites or ion couples are used to replace the activities a_i of components in the LF refining slags.

4. *Choosing standard molar Gibbs free energy changes of formed complex molecules*

Generally, the standard molar Gibbs free energy changes of reactions for forming any complex molecules should be cited at the liquid state. Taking the formation of the complex molecule $3CaO{\cdot}SiO_2$ as an example, the formation reaction of $3CaO{\cdot}SiO_2$ in Table V should be presented as follows:

$$3\left(Ca^{2+} + O^{2-}\right) + (SiO_2) = (3CaO \cdot SiO_2) \qquad [7a]$$

However, the melting points of most components in the slags, except FeO, are much higher than the common metallurgical operation temperature. In addition, the data of standard molar Gibbs free energy changes for dissolving these liquid components into the slags are scarce or absent from the related literatures. It is well known that dissolving or melting solid components into the slags can be divided into two subprocesses: one is melting or fusing the components from solid to liquid, and the other is dissolution of the liquid components into the slags.

The melting process and the related standard molar Gibbs free energy changes for melting $(Ca^{2+} + O^{2-})(s)$, $(SiO_2)(s)$ and $(3CaO{\cdot}SiO_2)(s)$ can be presented as follows:

$$\left(Ca^{2+} + O^{2-}\right)(s) = \left(Ca^{2+} + O^{2-}\right)(l) \qquad [8a]$$

$$\Delta_{fus} G_{m,CaO}^{\Theta} = \mu_{CaO(l)}^{*} - \mu_{CaO(s)}^{*} \quad (J/mol) \qquad [8b]$$

$$SiO_2(s) = SiO_2(l) \qquad [9a]$$

$$\Delta_{fus} G_{m,SiO_2}^{\Theta} = \mu_{SiO_2(l)}^{*} - \mu_{SiO_2(s)}^{*} \quad (J/mol) \qquad [9b]$$

$$3CaO \cdot SiO_2(s) = 3CaO \cdot SiO_2(l) \qquad [10a]$$

$$\Delta_{fus} G_{m,3CaO\cdot SiO_2}^{\Theta} = \mu_{3CaO\cdot SiO_2(l)}^{*} - \mu_{3CaO\cdot SiO_2(s)}^{*} \quad (J/mol) \qquad [10b]$$

It should be emphasized that the melting or fusing process has no standard state.

Based on pure solid matter as a standard state for structural units or components in the slags, the dissolution process and the related standard molar Gibbs free energy changes for dissolving $(Ca^{2+} + O^{2-})(l)$, $(SiO_2)(l)$ and $(3CaO{\cdot}SiO_2)(l)$ into the slags as $(Ca^{2+} + O^{2-})$, (SiO_2), and $(3CaO{\cdot}SiO_2)$ can be presented as

$$\left(Ca^{2+} + O^{2-}\right)(l) = \left(Ca^{2+} + O^{2-}\right) \qquad [11a]$$

$$\begin{aligned}\Delta_{sol} G_{m.CaO}^{\Theta} &= \mu_{CaO}^{\Theta} - \mu_{CaO(l)}^{*} \\ &= \mu_{CaO(s)}^{*} - \mu_{CaO(l)}^{*} \quad [50,51] \quad (J/mol)\end{aligned} \qquad [11b]$$

$$SiO_2(l) = (SiO_2) \qquad [12a]$$

$$\begin{aligned}\Delta_{sol} G_{m.SiO_2}^{\Theta} &= \mu_{SiO_2}^{\Theta} - \mu_{SiO_2(l)}^{*} \\ &= \mu_{SiO_2(s)}^{*} - \mu_{SiO_2(l)}^{*} \quad [50,51] \quad (J/mol)\end{aligned} \qquad [12b]$$

$$3CaO \cdot SiO_2(l) = (3CaO \cdot SiO_2) \qquad [13a]$$

$$\begin{aligned}&\Delta_{sol} G_{m,3CaO\cdot SiO_2}^{\Theta} \\ &= \mu_{3CaO\cdot SiO_2}^{\Theta} - \mu_{3CaO\cdot SiO_2(l)}^{*} \\ &= \mu_{3CaO\cdot SiO_2(s)}^{*} - \mu_{3CaO\cdot SiO_2(l)}^{*} \quad [50,51] \quad (J/mol)\end{aligned} \qquad [13b]$$

Comparing Eqs. [8b] through [10b] with Eqs. [11b] through [13b], the following equations can be obtained relative to the pure solid matter as a standard state for all structural units or components in the slags as

$$\Delta_{sol} G_{m,CaO}^{\Theta} = -\Delta_{fus} G_{m,CaO}^{\Theta} \quad (J/mol) \qquad [14a]$$

$$\Delta_{sol} G_{m,SiO_2}^{\Theta} = -\Delta_{fus} G_{m,SiO_2}^{\Theta} \quad (J/mol) \qquad [14b]$$

$$\Delta_{sol} G_{m,3CaO\cdot SiO_2}^{\Theta} = -\Delta_{fus} G_{m,3CaO\cdot SiO_2}^{\Theta} \quad (J/mol) \qquad [14c]$$

Therefore, the value of the standard molar Gibbs free energy change of melting or fusing component i from a solid into liquid $\Delta_{fus} G_{m,i}^{\Theta}$ is equal to the opposite value for the standard molar Gibbs free energy change of dissolving the liquid component i into the slags $\Delta_{sol} G_{m,i}^{\Theta}$ relative to the pure solid as a standard state.

The standard molar Gibbs free energy change of reaction for forming $3CaO{\cdot}SiO_2(s)$ by CaO(s) and

SiO_2(s) can be found from the related literature[35] as

$$3\left(Ca^{2+} + O^{2-}\right)(s) + (SiO_2)(s) = (3CaO \cdot SiO_2)(s) \quad [15a]$$

$$\Delta_r G^{\Theta}_{m,3CaO\cdot SiO_2(s)} = -118826 - 6.694T^{[35]} \quad (J/mol) \quad [15b]$$

The standard molar Gibbs free energy change for reaction in Eq. [7a] in liquid can be derived by combining Eqs. [8b] through [15b] as follows:

$$\begin{aligned}\Delta_r G^{\Theta}_{m,3CaO\cdot SiO_2} &= \Delta_r G^{\Theta}_{m,3CaO\cdot SiO_2(s)} - 3\Delta_{fus} G^{\Theta}_{m,CaO} - \Delta_{fus} G^{\Theta}_{m,SiO_2} \\ &+ \Delta_{fus} G^{\Theta}_{m,3CaO\cdot SiO_2} - 3\Delta_{sol} G^{\Theta}_{m,CaO} - \Delta_{sol} G^{\Theta}_{m,SiO_2} \\ &+ \Delta_{sol} G^{\Theta}_{m,3CaO\cdot SiO_2} = \Delta_r G^{\Theta}_{m,3CaO\cdot SiO_2(s)} \\ &= -118826 - 6.694T \quad (J/mol) \end{aligned} \quad [7b]$$

The expression of ion couple $(Ca^{2+} + O^{2-})$ in Eqs. [7a] and [11a] has the same meaning with the dissolved CaO in slags as (CaO), rather than pure liquid CaO, *i.e.*, $(Ca^{2+} + O^{2-})$(l) according to IMCT[29–33] or CaO(l). Therefore, the standard molar Gibbs free energy change $\Delta_r G^{\Theta}_{m,3CaO\cdot SiO_2}$ for reaction in Eq. [7a] has the same value or formula as $\Delta_r G^{\Theta}_{m,3CaO\cdot SiO_2(s)}$ for reaction in Eq. [15a] based on pure solid matter as a standard state for the calculated N_i.

Using the same deduction method, it can be also proved that the standard molar Gibbs free energy change for $(Mg^{2+} + O^{2-})(s) + (SiO_2)(s) = (MgO\cdot SiO_2)(l)$ in Table V has the same value for $(Mg^{2+} + O^{2-}) + (SiO_2) = (MgO\cdot SiO_2)$.

These results suggest that the standard molar Gibbs free energy change of the related reactions for the formation of complex molecules in Table V will not change by representing a solid or liquid as their existing state for reactants and products at the LF refining temperature for the defined N_i relative to the pure solid or liquid matter as a standard state according to IMCT.[29–33]

C. *Results of Mass Action Concentrations of Structural Units or Ion Couples in LF Refining Slags*

1. *Relation between mass percentage of six components and equilibrium mole numbers of related structural units or ion couples in LF refining slags*

The relationship between the mass percentage of CaO, SiO_2, MgO, FeO, MnO, and Al_2O_3 as components and the calculated equilibrium mole number of $(Ca^{2+} + O^{2-})$, SiO_2, $(Mg^{2+} + O^{2-})$ $(Fe^{2+} + O^{2-})$, $(Mn^{2+} + O^{2-})$, and Al_2O_3 as ion couples or structural units in CaO–SiO_2–MgO–FeO–MnO–Al_2O_3 slags at initial, middle, and final stages during 21 test runs of a 210-ton LF refining process is shown in Figure 2, respectively. The calculated $2n_{CaO}$, $2n_{FeO}$, $2n_{MnO}$, and $n_{Al_2O_3}$ has an obvious linear relationship with the mass percentage of CaO, FeO, MnO, and Al_2O_3, respectively; however, the scattered relations between n_i and (pct i) for both SiO_2 and MgO can be observed in Figures 2(b) and (c) simultaneously. The scattered relation for SiO_2 as structural unit in Figure 2(b) can be

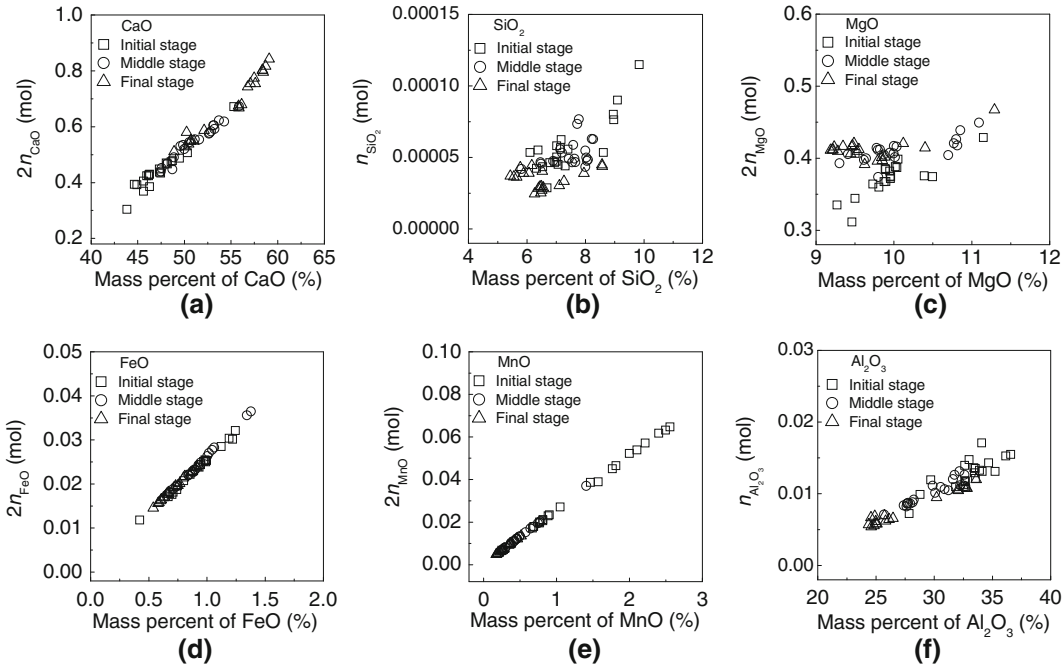

Fig. 2—Relationship between mass percentage of CaO, SiO_2, MgO, FeO, MnO, and Al_2O_3 as components and calculated mole number of $(Ca^{2+} + O^{2-})$, SiO_2, $(Mg^{2+} + O^{2-})$, $(Fe^{2+} + O^{2-})$, $(Mn^{2+} + O^{2-})$, and Al_2O_3 as ion couples or structural units in CaO–SiO_2–MgO–FeO–MnO–Al_2O_3 slags at initial, middle, and final stages during 21 test runs of a 210-ton LF refining process, respectively.

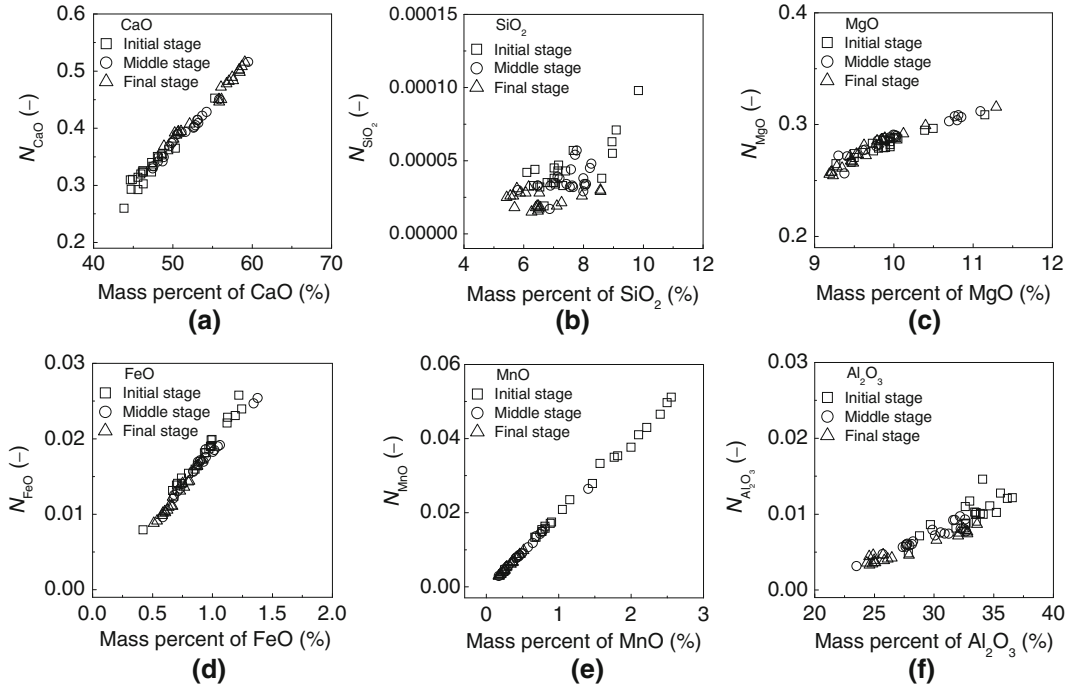

Fig. 3—Relationship between mass percentage of CaO, SiO_2, MgO, FeO, MnO and Al_2O_3 as components and mass action concentration of $(Ca^{2+} + O^{2-})$, SiO_2, $(Mg^{2+} + O^{2-})$, $(Fe^{2+} + O^{2-})$, $(Mn^{2+} + O^{2-})$, and Al_2O_3 as ion couples or structural units in CaO–SiO_2–MgO–FeO–MnO–Al_2O_3 slags at initial, middle, and final stages during 21 test runs of a 210-ton LF refining process, respectively.

explained as most of the structural unit SiO_2 can be bonded as $2CaO{\cdot}SiO_2$, $3CaO{\cdot}SiO_2$, $CaO{\cdot}SiO_2$, *etc.* at the metallurgical temperature as listed in Tables IV and V. The SiO_2 content is in a low range of 5–10 pct in the LF refining slags, whereas n_{SiO_2} is small in a range of 0.5×10^{-4} to 1.0×10^{-4} mol, compared with the average value of Σn_i as 1.315, 1.428, and 1.505 mol in 100 g of the slags at the initial, middle, and final stage as listed in Tables I through III, respectively. Some interesting results for the ion couple $(Mg^{2+} + O^{2-})$ can be obtained from Figure 2(c) that (a) $2n_{MgO}$ and (pct MgO) has a good corresponding relation at the initial stage in the slags; (b) a relative constant $2n_{MgO}$ of about approximately 0.4 mol can be observed in a narrow (pct MgO) range of 9–10 pct at the middle and final stage in 100-g of the slags for some test runs. These test runs correspond to increasing (pct CaO) from 49 pct to 58 pct, decreasing (pctAl_2O_3) from 33 pct to 26 pct, maintaining (pct MgO) constant as 9–10 pct, increasing Σn_i from 1.435 mol to 1.475 mol in 100-g of the slags for related test runs in No. 16 through No. 20 at middle stage, or increasing Σn_i from 1.495 mol to 1.633 mol in 100-g of the slags for related test runs in No. 1 and No. 12 through No. 20 at the final stage by choosing the No. 9 test run as a basis at both the middle and final stages, respectively.

2. *Relation between mass percentage of six components and mass action concentrations of related structural units or ion couples in LF refining slags*

The relationship between the mass percentage of CaO, SiO_2, MgO, FeO, MnO, and Al_2O_3 as components and the calculated mass action concentration of $(Ca^{2+} + O^{2-})$, SiO_2, $(Mg^{2+} + O^{2-})$ $(Fe^{2+} + O^{2-})$, $(Mn^{2+} + O^{2-})$ and Al_2O_3 as ion couples or structural units in CaO–SiO_2–MgO–FeO–MnO–Al_2O_3 slags at the initial, middle, and final stages during 21 test runs of a 210-ton LF refining process is shown in Figure 3, respectively. It can be observed from Figure 3 that (pct CaO), (pct MgO), (pct FeO) and (pct MnO) has an obvious linear relationship with N_{CaO}, N_{MgO}, N_{FeO}, and N_{MnO} respectively, whereas the scattered relations between N_i and (pct i) for SiO_2 and Al_2O_3 can be observed in Figures 3(b) and (f) because the generated complex molecules contain SiO_2 and Al_2O_3 simultaneously as listed in Tables IV and V.

3. *Relation between equilibrium mole numbers and mass action concentrations for structural units or ion couples in LF refining slags*

The relationship between the equilibrium mole number n_i and the mass action concentration N_i for 31 structural units or ion couples, *i.e.,* 5 ion couples, 2 simple molecules, and 24 complex molecules in the CaO–SiO_2–MgO–FeO–MnO–Al_2O_3 slags except ion couples $(Mg^{2+} + S^{2-})$, $(Fe^{2+} + S^{2-})$, and $(Mn^{2+} + S^{2-})$ at the initial, middle, and final stages during 21 test runs of a 210-ton LF refining process is shown in Figure 4, respectively. It is shown clearly in Figure 4 that n_i and N_i for 30 structural units or ion couples have an obvious linear relationship except the ion couple $(Mg^{2+} + O^{2-})$ or free MgO. The slope of linear relationship can be treated as the reciprocal of Σn_i, *i.e.*, $1/\Sigma n_i$ when the intercept of the corresponding linear relationship is small enough according to Eqs. [2] and [3] for 30 structural units or ion couples. The nonlinear relationship between $2n_{MgO}$ and N_{MgO} at both the middle and

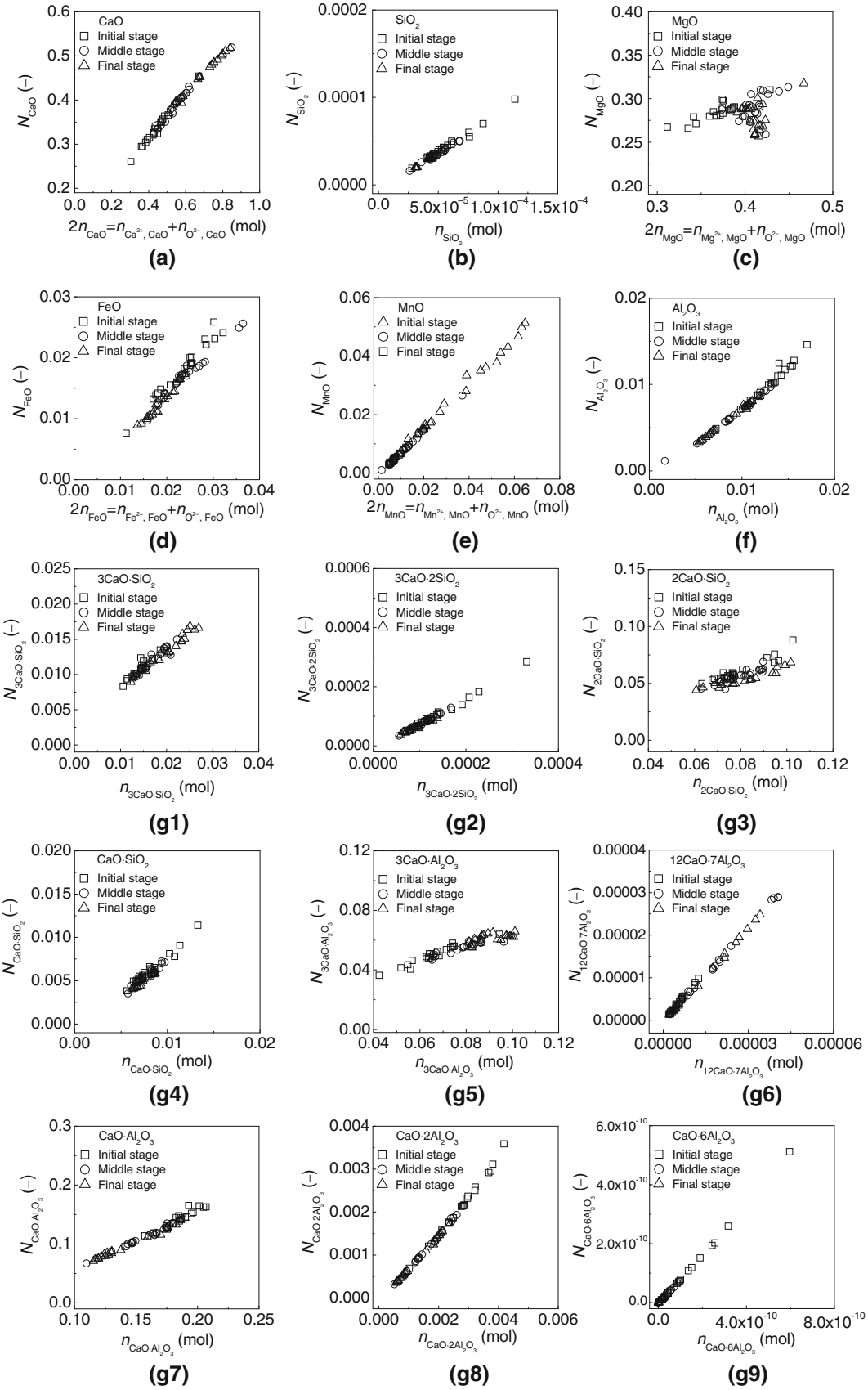

Fig. 4—Relationship between calculated equilibrium mole number and mass action concentration of structural units or ion couples in CaO–SiO_2–MgO–FeO–MnO–Al_2O_3 slags at initial, middle, and final stages during 21 test runs of a 210-ton LF refining process, respectively.

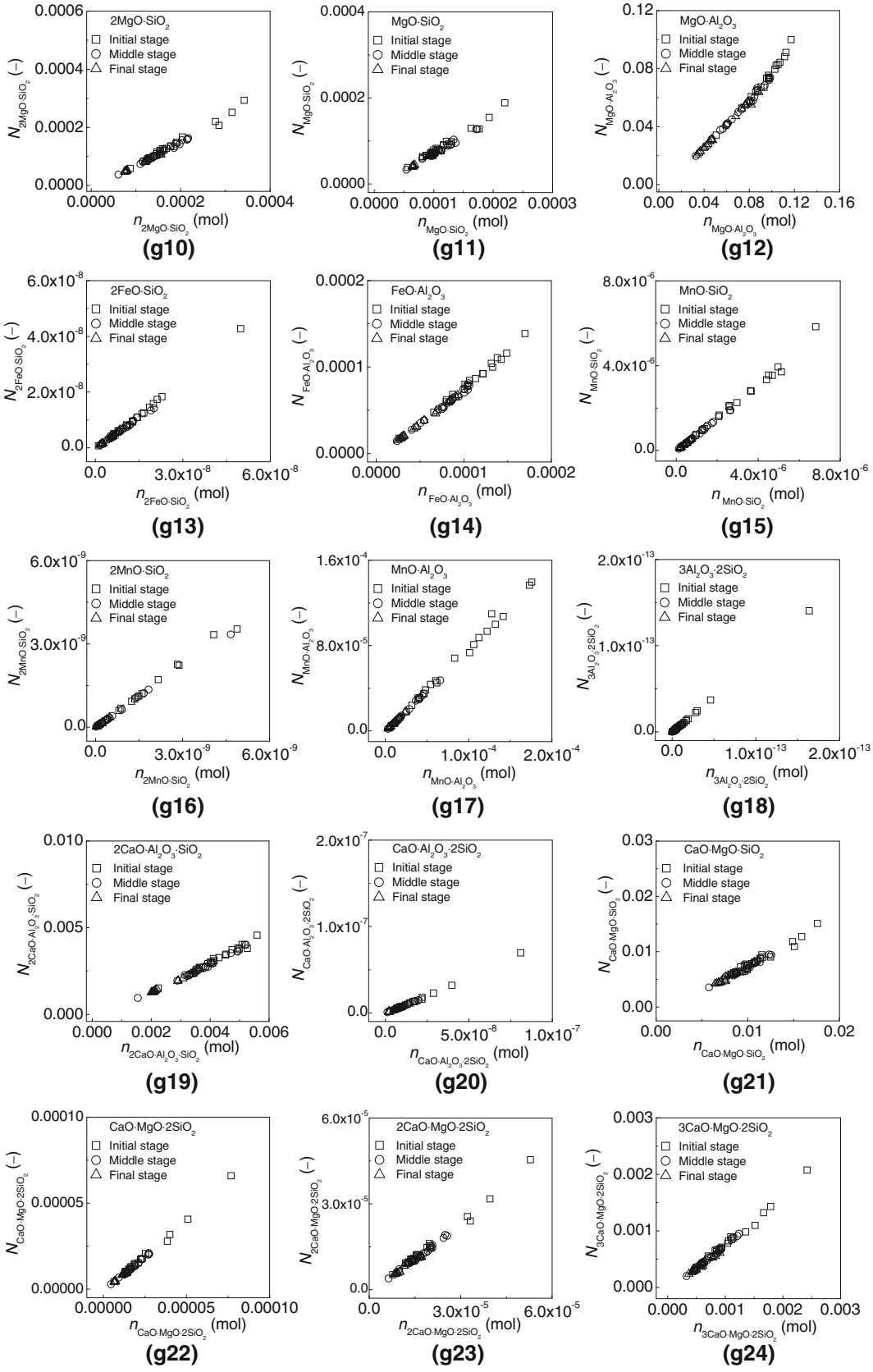

Fig. 4—continued.

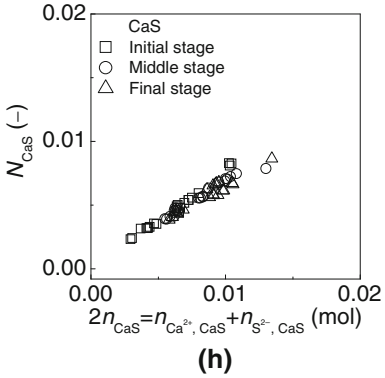

Fig. 4—continued.

final stages can be explained from the results shown in Figure 2(c) that maintaining $2n_{MgO}$ in a narrow range of 0.39–0.41 mol corresponds to an increasing of Σn_i from 1.30 mol to 1.46 mol at the middle stage and Σn_i from 1.4 mol to 1.6 mol at the final stage caused by increasing (pct CaO) from 49 pct to 58 pct and decreasing (pct Al_2O_3) from 33 pct to 26 pct, keeping (pct MgO) constant as 9–10 pct in the slags for the related test runs. Therefore, N_{MgO} shows a vertical decreasing tendency in these test runs at middle and final stages as shown in Figure 4(c).

Comparing Figures 2 and 3, it can be deduced that although a great amount of SiO_2 or Al_2O_3 can be bonded as complex molecules as listed in Tables IV and V, the bonded amount of SiO_2 or Al_2O_3 cannot affect the relation between n_i and N_i for free SiO_2 or free Al_2O_3 as structural unit in the slags during LF refining process.

The calculated results indicate that the calculated equilibrium mole number n_i of structural units or ion couples and calculated mass action concentration N_i of structural units or ion couples, rather than the mass percent of components (pct i), are recommended to represent the real concentration of components in the $CaO–SiO_2–MgO–FeO–MnO–Al_2O_3$ slags equilibrated or reacted with molten steel during LF refining process.

IV. MODEL FOR CALCULATING SULFUR DISTRIBUTION RATIO BETWEEN LF REFINING SLAGS AND MOLTEN STEEL

A. *Establishment of Sulfur Distribution Ratio Model*

Similar to the viewpoint from classically metallurgical physicochemistry that only basic oxides or components in slags have desulfurization potential, ion couples $(Ca^{2+}+O^{2-})$, $(Mg^{2+}+O^{2-})$, $(Fe^{2+}+O^{2-})$, and $(Mn^{2+}+O^{2-})$ can take roles in the desulfurization reactions and provide desulfurization potential in the LF refining slags according to IMCT.[29–33] The desulfurization reactions of ion couples $(Ca^{2+}+O^{2-})$, $(Mg^{2+}+O^{2-})$, $(Fe^{2+}+O^{2-})$, and $(Mn^{2+}+O^{2-})$ in the LF refining slags from molten steel, and their standard molar Gibbs free energy changes are presented as follows:

$$\left(Ca^{2+}+O^{2-}\right)+[S]=\left(Ca^{2+}+S^{2-}\right)+[O]$$
$$\Delta_r G^{\Theta}_{m,CaS}=105784.6-28.723T^{[52,53]}\quad (J/mol) \qquad [16a]$$

$$\left(Mg^{2+}+O^{2-}\right)+[S]=\left(Mg^{2+}+S^{2-}\right)+[O]$$
$$\Delta_r G^{\Theta}_{m,MgS}=203604.6-35.023T^{[53,54]}\quad (J/mol) \qquad [16b]$$

$$\left(Fe^{2+}+O^{2-}\right)+[S]=\left(Fe^{2+}+S^{2-}\right)+[O]$$
$$\Delta_r G^{\Theta}_{m,FeS}=115526-33.352T^{[27,55,56]}\quad (J/mol) \qquad [16c]$$

$$\left(Mn^{2+}+O^{2-}\right)+[S]=\left(Mn^{2+}+S^{2-}\right)+[O]$$
$$\Delta_r G^{\Theta}_{m,MnS}=83956-30.78T^{[28,55,56]}\quad (J/mol) \qquad [16d]$$

Based on the calculated N_{CaO}, N_{MgO}, N_{FeO}, and N_{MnO}, the definition of N_{CaS}, N_{MgS}, N_{FeS}, and N_{MnS}, the oxygen activity a_O, and the sulfur activity a_S of molten steel, the equilibrium constant of desulfurization reactions shown in Eq. [16] can be expressed as follows:

$$K^{\Theta}_{CaS}=\frac{a_{CaS}a_O}{a_{CaO}a_S}=\frac{N_{CaS}a_O}{N_{CaO}a_S}=\frac{\left(2(\text{pct S})_{CaS}/M_S/\sum n_i\right)[\text{pct O}]f_O}{N_{CaO}[\text{pct S}]f_S}=\frac{(\text{pct S})_{CaS}[\text{pct O}]}{16N_{CaO}[\text{pct S}]\sum n_i}\times\frac{f_O}{f_S}\quad (-) \qquad [17a]$$

$$K^{\Theta}_{MgS}=\frac{a_{MgS}a_O}{a_{MgO}a_S}=\frac{N_{MgS}a_O}{N_{MgO}a_S}=\frac{\left(2(\text{pct S})_{MgS}/M_S/\sum n_i\right)[\text{pct O}]f_O}{N_{MgO}[\text{pct }S]f_S}=\frac{(\text{pct S})_{MgS}[\text{pct O}]}{16N_{MgO}[\text{pct S}]\sum n_i}\times\frac{f_O}{f_S}\quad (-) \qquad [17b]$$

$$K^{\Theta}_{FeS}=\frac{a_{FeS}a_O}{a_{FeO}a_S}=\frac{N_{FeS}a_O}{N_{FeO}a_S}=\frac{\left(2(\text{pct S})_{FeS}/M_S/\sum n_i\right)[\text{pct O}]f_O}{N_{FeO}[\text{pct S}]f_S}=\frac{(\text{pct S})_{FeS}[\text{pct O}]}{16N_{FeO}[\text{pct S}]\sum n_i}\times\frac{f_O}{f_S}\quad (-) \qquad [17c]$$

$$K^{\Theta}_{MnS}=\frac{a_{MnS}a_O}{a_{MnO}a_S}=\frac{N_{MnS}a_O}{N_{MnO}a_S}=\frac{\left(2(\text{pct S})_{MnS}/M_S/\sum n_i\right)[\text{pct O}]f_O}{N_{MnO}[\text{pct S}]f_S}=\frac{(\text{pct S})_{MnS}[\text{pct O}]}{16N_{MnO}[\text{pct S}]\sum n_i}\times\frac{f_O}{f_S}\quad (-) \qquad [17d]$$

where M_S is the atomic mass of sulfur element of 32 (–). Therefore, the respective sulfur distribution ratio of the ion couple $(Ca^{2+}+O^{2-})$, $(Mg^{2+}+O^{2-})$, $(Fe^{2+}+O^{2-})$, and $(Mn^{2+}+O^{2-})$ in the LF refining

slags equilibrated or reacted with molten steel can be deduced from Eqs. [17a] through [17d] as

$$L_{S,CaO} = \frac{(\text{pct S})_{CaS}}{[\text{pct S}]} = \frac{16K^{\Theta}_{CaS}N_{CaO}\sum n_i}{[\text{pct O}]} \times \frac{f_S}{f_O} \quad (-) \qquad [18a]$$

$$L_{S,MgO} = \frac{(\text{pct S})_{MgS}}{[\text{pct S}]} = \frac{16K^{\Theta}_{MgS}N_{MgO}\sum n_i}{[\text{pct O}]} \times \frac{f_S}{f_O} \quad (-) \qquad [18b]$$

$$L_{S,FeO} = \frac{(\text{pct S})_{FeS}}{[\text{pct S}]} = \frac{16K^{\Theta}_{FeS}N_{FeO}\sum n_i}{[\text{pct O}]} \times \frac{f_S}{f_O} \quad (-) \qquad [18c]$$

$$L_{S,MnO} = \frac{(\text{pct S})_{MnS}}{[\text{pct S}]} = \frac{16K^{\Theta}_{MnS}N_{MnO}\sum n_i}{[\text{pct O}]} \times \frac{f_S}{f_O} \quad (-) \qquad [18d]$$

The activity coefficient of sulfur and the dissolved oxygen in molten steel, f_S and f_O, at 1873 K (1600 °C) can be calculated by Wagner's equation as follows:

$$\lg f_i = \sum e^j_i[\text{pct } j] \quad (-) \qquad [19a]$$

where e^j_i is the activity interaction coefficient of element j to i in molten steel based on the mass percentage as a concentration unit and one mass percent (1 pct) as standard state (–). The effect of temperature on activity interaction coefficient e^j_i can be expressed by

$$e^j_i = \frac{A}{T} + B \quad (-) \qquad [19b]$$

where A and B are different constants[57] for various elements j and i in molten steel (–). Because e^j_i has a little change with temperature variation in metallurgical temperature range, values of e^j_i chosen from literature[57] at 1873 K (1600 °C) are summarized as $e^C_O = -0.45$, $e^{Si}_O = -0.131$, $e^{Mn}_O = -0.021$, $e^P_O = -0.07$, $e^S_O = -0.133$, $e^{Al}_O = -3.9$, $e^S_S = -0.028$, $e^c_S = 0.11$, $e^{Si}_S = 0.063$, $e^{Mn}_S = -0.026$, $e^P_S = 0.29$, and $e^{Al}_S = 0.035$. Certainly, the LF refining temperature in a range from 1800 K to 1935 K (1527 °C to 1662 °C) as listed in Tables I through III has a small gap with the reported e^j_i[57] at 1873 K (1600 °C).

The total sulfur distribution ratio between the LF refining slags and molten steel is equal to the sum of the respective sulfur distribution ratio of all ion couples with the desulfurization potential in the slags as

$$\begin{aligned} L_S &= L_{S,CaO} + L_{S,MgO} + L_{S,FeO} + L_{S,MnO} \\ &= \frac{(\text{pct S})_{CaS} + (\text{pct S})_{MgS} + (\text{pct S})_{FeS} + (\text{pct S})_{MnS}}{[\text{pct S}]} \\ &= \frac{16\left(K^{\Theta}_{CaS}N_{CaO} + K^{\Theta}_{MgS}N_{MgO} + K^{\Theta}_{FeS}N_{FeO} + K^{\Theta}_{MnS}N_{MnO}\right)\sum n_i}{[\text{pct O}]} \times \frac{f_S}{f_O} \\ &= \frac{16\left(K^{\Theta}_{CaS}N_{CaO} + K^{\Theta}_{MgS}N_{MgO} + K^{\Theta}_{FeS}N_{FeO} + K^{\Theta}_{MnS}N_{MnO}\right)f_S\sum n_i}{a_O} \quad (-) \end{aligned} \qquad [20]$$

Therefore, the total sulfur distribution ratio L_S between LF refining slags and molten steel, as well as the respective sulfur distribution ratio $L_{S,CaO}$, $L_{S,MgO}$, $L_{S,FeO}$, and $L_{S,MnO}$ of ion couples $(Ca^{2+} + O^{2-})$, $(Mg^{2+} + O^{2-})$, $(Fe^{2+} + O^{2-})$, and $(Mn^{2+} + O^{2-})$ in the slags equilibrated or reacted with molten steel can be calculated after knowing the values of K^{Θ}_{CaS}, K^{Θ}_{MgS}, K^{Θ}_{FeS}, K^{Θ}_{MnS}, N_{CaO}, N_{MgO}, N_{FeO}, N_{MnO}, and $\sum n_i$, as well as the oxygen activity of a_O and f_S. Certainly, the chemical composition of the slags can affect N_{CaO}, N_{MgO}, N_{FeO}, and, N_{MnO} when K^{Θ}_{CaS}, K^{Θ}_{MgS}, K^{Θ}_{FeS}, and K^{Θ}_{MnS} are determined by temperature T through $\Delta_r G^{\Theta}_{m,CaS}$, $\Delta_r G^{\Theta}_{m,MgS}$, $\Delta_r G^{\Theta}_{m,FeS}$, and $\Delta_r G^{\Theta}_{m,MnS}$. The magnitude of N_{CaO}, N_{MgO}, N_{FeO}, andN_{MnO} has been given in Figure 4. The equilibrium mole number Σn_i of all structural units in 100-g slags is almost a constant as 1.315, 1.428, and 1.505 at the initial, middle, and final stages as listed in Tables I through III.

In addition, ignoring the sulfur boned with ion couples $(Mg^{2+} + O^{2-})$, $(Fe^{2+} + O^{2-})$, and $(Mn^{2+} + O^{2-})$ as ion couples $(Mg^{2+} + S^{2-})$, $(Fe^{2+} + S^{2-})$, and $(Mn^{2+} + S^{2-})$ in the slags described in Sections III–A and III–B. *i.e.*, $b_8 = n^0_{MgS} \approx 0$, $b_9 = n^0_{Fes} \approx 0$, and $b_{10} = n^0_{MnS} \approx 0$, can generate a small deviation on $L_{S,CaO}$, $L_{S,MgO}$, $L_{S,FeO}$, $L_{S,MnO}$, and L_S by affecting N_{CaO}, N_{MgO}, N_{FeO}, N_{MnO}, and $\sum n_i$ in Eqs. [18] and [20]. However, it cannot affect the rationality of the defined $L_{S,MgO}$, $L_{S,FeO}$, and$L_{S,MnO}$ as shown in Eqs. [18b] through [18d]. This means that assuming the sulfur bonded as $(Mg^{2+} + S^{2-})$, $(Fe^{2+} + S^{2-})$, and $(Mn^{2+} + S^{2-})$ in the slags equilibrated or reacted with molten steel as zero cannot destroy the logical rationality of the defined $L_{S,MgO}$, $L_{S,FeO}$, $L_{S,MnO}$, and L_S in this study. The equilibrium reaction constants K^{Θ}_{CaS}, K^{Θ}_{MgS}, K^{Θ}_{FeS}, and K^{Θ}_{MnS} can be determined from $\Delta_r G^{\Theta}_{m,CaS}$, $\Delta_r G^{\Theta}_{m,MgS}$, $\Delta_r G^{\Theta}_{m,FeS}$, and $\Delta_r G^{\Theta}_{m,MnS}$ shown in Eq. [16] by

$$K^{\Theta}_i = \exp\left(-\Delta_r G^{\Theta}_{m,i}/RT\right) \quad (-) \qquad [21]$$

The sulfur activity coefficient f_S can be calculated by Eq. [19] after knowing the chemical composition and temperature of molten steel. As an important parameter of oxygen activity in the developed IMCT model shown in Eqs. [18] and [20], determining the oxygen activity of molten steel, especially the oxygen activity of molten steel at the slag–metal interface or beneath the slag–metal interface, is an important and challenging task to apply the developed thermodynamic model for calculating sulfur distribution ratio between the LF refining slags and molten steel based on IMCT.[29–33] This will be described in detail in the next section.

B. *Determination of Oxygen Activity of Bulk Molten Steel and Molten Steel at Slag–Metal Interface*

It is well known that the desulfurization reaction occurs at the slag–metal interface during LF refining process and can be expressed by ion exchange reaction as

$$\left(O^{2-}\right) + [S] = \left(S^{2-}\right) + [O] \qquad [22]$$

Obviously, higher oxygen ion activity $a_{O^{2-}}$ in slags and the lower oxygen activity $a_{O,interface}$ of molten steel beneath slag–metal interface are two beneficial factors to promote the desulfurization reaction in Eq. [22]. Although the oxygen activity of the molten steel has been measured *in situ* by an oxygen sensor below the slag–metal interface of 0.3 m, no industrial experiences or published literatures can confirm that the measured oxygen activity of bulk molten steel by an oxygen sensor can represent the oxygen activity of molten steel at the slag–metal interface. Therefore, four methods of determining the oxygen activity, *i.e.,* the measured oxygen activity by an oxygen sensor, the calculated oxygen activity based on [Al]–[O] equilibrium in bulk molten steel with assuming $a_{Al_2O_3}$ as 1, the calculated oxygen activity based on (Al_2O_3)–[O] equilibrium at the slag–metal interface considering the Al_2O_3 activity $a_{Al_2O_3}$ as that in the slags, and the calculated oxygen activity based on the (FeO)–[O] equilibrium at the slag–metal interface considering the FeO activity a_{Feo} as that in the slags, have been used to calculate the sulfur distribution ratio by the developed IMCT model. Comparing the measured and the calculated sulfur distribution ratio by applying different oxygen activities by the previously mentioned methods can confirm which method of determining the oxygen activity can determine the ideal oxygen activity of molten steel at the slag–metal interface.

1. *Comparison of oxygen activity of bulk molten steel based on [Al]–[O] equilibrium and measured oxygen activity by oxygen sensor*

The LF refining process proceeds under the condition of molten steel deoxidized or killed by aluminum as well as strong stirred by bottom blowing Ar gas. Under these circumstances, the dissolved oxygen content or oxygen activity in bulk molten steel will be equilibrated and controlled with aluminum content as follows:

$$2[Al] + 3[O] = (Al_2O_3)(s)$$

$$\Delta_r G^{\Theta}_{m,Al_2O_3,s} = -1202000 + 386.30T^{[57-60]} \quad (J/mol) \qquad [23]$$

Oxygen activity $a_{O,[Al]-[O]}$ of bulk molten steel based on the [Al]–[O] equilibrium can be calculated from Eq. [23] as

$$a_{O,[Al]-[O]} = \left[\frac{a_{Al_2O_3,s}}{a_{Al}^2 \exp\left(-\Delta_r G^{\Theta}_{m,Al_2O_3,s}/RT\right)}\right]^{1/3} \quad (-) \qquad [24]$$

where a_{Al} is the activity of [Al] in molten steel (–) and $a_{Al_2O_3,s}$ is the activity of solid Al_2O_3 in molten steel as unity, *i.e.*, 1. The activity of [Al] in the molten steel a_{Al} can be calculated by

$$a_{Al} = f_{Al}[\text{pct Al}] \quad (-) \qquad [25]$$

The activity coefficient of the aluminum f_{Al} in molten steel can be calculated by Wagner's equation in Eq. [19a] by taking values of the related aluminum activity interaction parameters as[57] $e^{C}_{Al} = 0.091$, $e^{Si}_{Al} = 0.0056$, $e^{Mn}_{Al} = 0.0$, $e^{P}_{Al} = 0.0$, $e^{S}_{Al} = 0.03$, and $e^{Al}_{Al} = 0.045$, respectively. It should be noted that the values of the aluminum activity interaction parameters e^{Mn}_{Al} and e^{P}_{Al} are assumed as zero for the lack of values in the related literatures.

The comparison of the calculated oxygen activity $a_{O,[Al]-[O]}$ based on the [Al]–[O] equilibrium assuming the Al_2O_3 activity $a_{Al_2O_3,s}$ as 1 and the measured oxygen activity $a_{O,sensor}$ by oxygen sensor of bulk molten steel at the initial, middle, and final stages during 21 test runs of a 210-ton LF refining process is illustrated in Figure 5, respectively. It can be observed that $a_{O,sensor}$ maintains a small value less than 10×10^{-4} during the entire LF refining process. A close corresponding relationship exists between the measured $a_{O,sensor}$ and $a_{O,[Al]-[O]}$, although there are some scattered data at the initial, middle, and final stages during the LF refining process, respectively. Therefore, it can be deduced that $a_{O,bath}$ of bulk molten steel with a lower value is controlled by the killed aluminum content [pct Al] and $a_{O,[Al]-[O]}$ can be used to represent the oxygen activity of the bulk molten steel $a_{O,bath}$ as the measured $a_{O,sensor}$ by the oxygen sensor.

2. *Comparison of oxygen activity of molten steel at slag–metal interface based on (Al_2O_3)–[O] equilibrium and measured oxygen activity by oxygen sensor*

Some researchers recommended[61–63] that the oxygen activity of molten steel at the slag–metal interface $a_{O,interface}$, rather than that of molten steel bulk $a_{O,bath}$, is more reasonable to represent the oxygen activity of molten steel at the slag–metal interface and to affect the desulfurization reactions seriously. Considering that the LF refining process proceeds with higher binary basicity of slags as well as lower $a_{O,bath}$ of molten steel, it is more logical that the $a_{O,interface}$ of molten steel at the slag–metal interface, *i.e.*, at desulfurization zone, is determined based on the equilibrium of species in molten steel and their corresponding oxides in slags. The equilibrium reaction between [O] in molten steel and Al_2O_3 in slags can be represented as

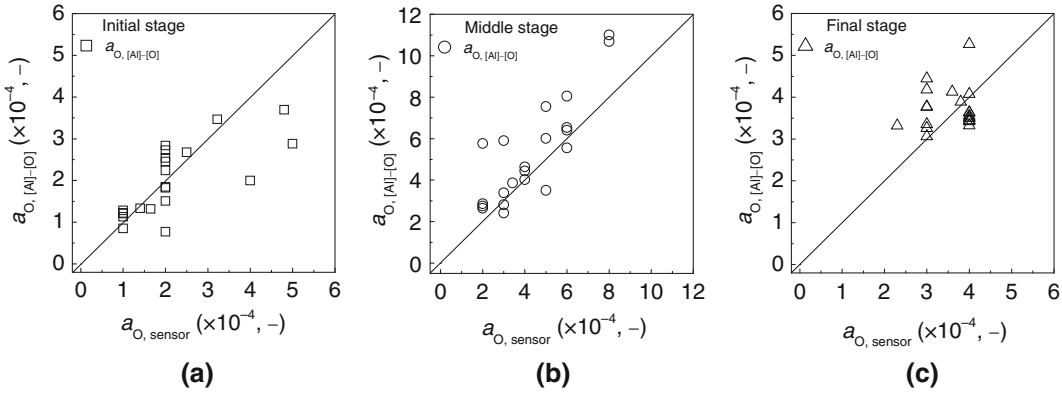

Fig. 5—Comparison of measured oxygen activity $a_{O,sensor}$ by the oxygen sensor and calculated oxygen activity $a_{O,[Al]-[O]}$ in bulk molten steel based on [Al]–[O] equilibrium by assuming Al_2O_3 activity $a_{Al_2O_3,s}$ as unity, *i.e.*, 1 at initial, middle, and final stages during 21 test runs of a 210-ton LF refining process, respectively.

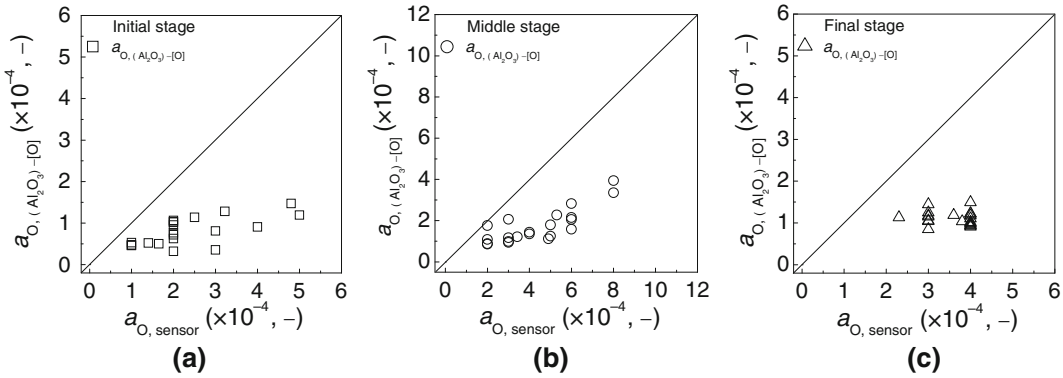

Fig. 6—Comparison of measured oxygen activity $a_{O,sensor}$ by the oxygen sensor and calculated oxygen activity $a_{O,(Al_2O_3)-[O]}$ of molten steel at the slag–metal interface based on (Al_2O_3)–[O] equilibrium by replacing Al_2O_3 activity $a_{Al_2O_3}$ by calculated mass action concentration $N_{Al_2O_3}$ of Al_2O_3 from IMCT at initial, middle, and final stages during 21 test runs of a 210-ton LF refining process, respectively.

$$2[Al] + 3[O] = (Al_2O_3)$$

$$\Delta_r G^{\Theta}_{m,Al_2O_3} = \Delta_r G^{\Theta}_{m,Al_2O_3,s} = -1202000 + 386.30T^{[57-60]} \quad (J/mol) \quad [26]$$

Therefore, the $a_{O,(Al_2O_3)-[O]}$ of molten steel at the desulfurization zone, *i.e.*, at slag–metal interface, can be calculated by

$$a_{O,(Al_2O_3)-[O]} = \left[\frac{a_{Al_2O_3}}{a_{Al}^2 \exp\left(-\Delta_r G^{\Theta}_{m,Al_2O_3}/RT\right)}\right]^{1/3} = \left[\frac{N_{Al_2O_3}}{a_{Al}^2 \exp\left(-\Delta_r G^{\Theta}_{m,Al_2O_3}/RT\right)}\right]^{1/3} \quad (-) \quad [27]$$

The activity of Al_2O_3 in slags $a_{Al_2O_3}$ can be calculated by the following empirical formula as[64]

$$\log a_{Al_2O_3} = \frac{[-0.275(\text{pct CaO}) + 0.167(\text{pct MgO})]}{(\text{pct SiO}_2)} + 0.033(\text{pct Al}_2\text{O}_3) - 1.560 \quad (-) \quad [28]$$

It should be emphasized that Eq. [28] can be only used to calculate $a_{Al_2O_3}$ in CaO–SiO_2–MgO–Al_2O_3 quaternary slags at 1873 K (1600 °C) without considering the effect of other components as well as temperature change on $a_{Al_2O_3}$. Certainly, there are some obvious limitations of Eq. [28] to accurately determine $a_{Al_2O_3}$ of the LF refining slags. Under this circumstance, the calculated $N_{Al_2O_3}$ is used to substitute $a_{Al_2O_3}$ in CaO–SiO_2–MgO–FeO–MnO–Al_2O_3 slags. The comparison between the calculated oxygen activity $a_{O,(Al_2O_3)-[O]}$ of molten steel at the slag–metal interface based on (Al_2O_3)–[O] equilibrium with replacing Al_2O_3 activity $a_{Al_2O_3}$ by $N_{Al_2O_3}$ from IMCT[29–33] and the measured $a_{O,sensor}$ of molten steel by oxygen sensor at the initial, middle, and final stages during 21 test runs of a 210-ton LF refining process is illustrated in Figure 6, respectively. It is shown from Figure 6 that the calculated $a_{O,(Al_2O_3)-[O]}$ based on the (Al_2O_3)–[O] equilibrium is much smaller than the measured $a_{O,sensor}$ by oxygen sensor because the calculated $N_{Al_2O_3}$ in Eq. [27] is in a range of 0.003152–0.014602, which is much smaller than $a_{Al_2O_3,s}$ as 1 in Eq. [24] with the same value of $\Delta_r G^{\Theta}_{m,Al_2O_3,s}$ in Eq. [23] and $\Delta_r G^{\Theta}_{m,Al_2O_3}$ in Eq. [26] relative to pure solid matter as a standard state and solid pure matter as a standard state.[50,51]

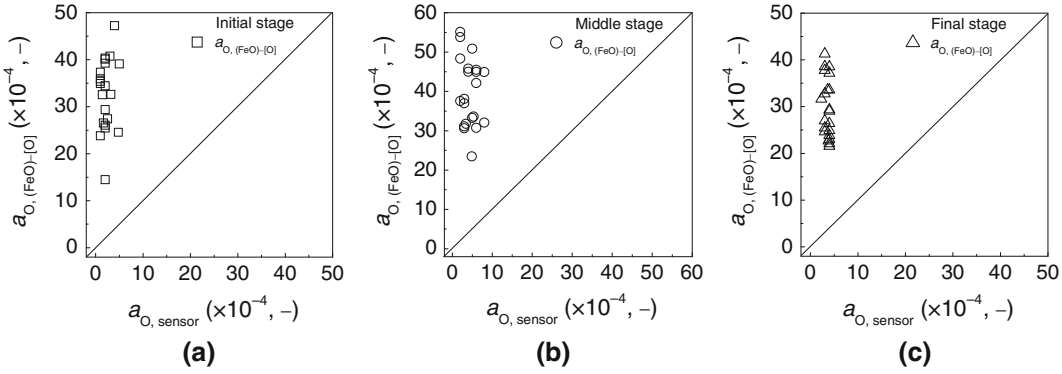

Fig. 7—Comparison of measured oxygen activity $a_{O,sensor}$ by the oxygen sensor and calculated oxygen activity $a_{O,(FeO)-[O]}$ of molten steel at the slag–metal interface based on (FeO)–[O] equilibrium by replacing FeO activity a_{FeO} by calculated mass action concentration of FeO N_{FeO} from IMCT at initial, middle, and final stages during 21 test runs of a 210-ton LF refining process, respectively.

3. *Comparison of oxygen activity of molten steel at slag–metal interface based on (FeO)–[O] equilibrium and measured oxygen activity by oxygen sensor*

For the same reason described in Section IV–B–2, the oxygen activity of molten steel at the slag–metal interface $a_{O,interface}$ can be also determined under the condition of [O] in molten steel equilibrated with FeO in the slags as follows:

$$[Fe] + [O] = (FeO)$$

$$\Delta_r G^{\Theta}_{m,FeO} = -117733.7 + 49.85T^{[65-66]} \quad (J/mol) \quad [29]$$

$a_{O,(FeO)-[O]}$ of molten steel at desulfurization zone, *i.e.*, at the slag–metal interface, can be calculated by

$$a_{O,(FeO)-[O]} = \frac{a_{FeO}}{a_{Fe}\exp\left(-\Delta_r G^{\Theta}_{m,FeO}/RT\right)}$$

$$\text{or} \quad \log\frac{a_{O,(FeO)-[O]}}{a_{FeO}} = \frac{-6150}{T} + 2.604 \quad (-) \quad [30]$$

where a_{Fe} is the activity of [Fe] in molten steel as 1 (–). Although many methods or empirical formulas can be used to calculate a_{FeO} in slags,[65,67,68] the calculated N_{FeO} from IMCT[29–33] is used to substitute a_{FeO} in this study. The comparison of the calculated $a_{O,(FeO)-[O]}$ of molten steel at the slag–molten interface based on (FeO)–[O] equilibrium with replacing a_{FeO} by N_{FeO} from IMCT[29–33] and the measured $a_{O,Sensor}$ by the oxygen sensor at the initial, middle, and final stages during 21 test runs of a 210-ton LF refining process is illustrated in Figure 7, respectively. It is shown in Figure 7 that the calculated $a_{O,(FeO)-[O]}$ based on the (FeO)–[O] equilibrium is much greater than the measured $a_{O,sensor}$ by the oxygen sensor. Therefore, it cannot be confirmed which one of $a_{O,[Al]-[O]}$, $a_{O,(Al_2O_3)-[O]}$, $a_{O,(FeO)-[O]}$, and $a_{O,sensor}$ can be used to represent $a_{O,interface}$, although $a_{O,sensor}$ is almost the same as $a_{O,[Al]-[O]}$ to present $a_{O,bath}$ at the initial, middle, and final stages during the LF refining process.

C. *Calculation of $L^{IMCT}_{S,calculated}$ by IMCT Model Using Different Oxygen Activities*

Three methods of calculating oxygen activity as described in Section IV–B, *i.e.*, $a_{O,[A1]-[O]}$, $a_{O,(Al_2O_3)-[O]}$, and $a_{O,(FeO)-[O]}$ to represent $a_{O,bath}$ or $a_{O,interface}$, have been used to calculate the sulfur distribution ratio between the LF refining slags and molten steel at the initial, middle, and final stages during 21 test runs of a 210-ton LF refining process, respectively. Certainly, the calculated $a_{O,[Al]-[O]}$ of bulk molten steel based on the [Al]–[O] equilibrium is treated the same as the measured $a_{O,sensor}$ by the oxygen sensor. It is necessary to compare the calculated $L^{IMCT}_{S,calculated}$ by the IMCT model based on the various calculated oxygen activities, *i.e.*, $a_{O,[Al]-[O]}$, $a_{O,(Al_2O_3)-[O]}$, and $a_{O,(FeO)-[O]}$ with the measured $L_{S,measured}$ for the same test runs to decide which method of determining the oxygen activity can be used to represent $a_{O,interface}$.

1. *Comparison of calculated $L^{[Al]-[O],IMCT}_{S,calculated}$ by IMCT model using $a_{O,[A1]-[O]}$ of bulk molten steel and measured $L_{S,measured}$*

The relationship between the calculated $L^{[Al]-[O],IMCT}_{S,calculated}$ by the IMCT model using $a_{O,[Al]-[O]}$ under the [Al]–[O] equilibrium with assuming $a_{Al_2O_3,s}$ as 1 and the measured $L_{S,measured}$ at the initial, middle, and final stages during 21 test runs of a 210-ton LF refining process is illustrated in Figure 8, respectively. It is observed from Figure 8 that the measured $L_{S,measured}$ is less than 50, 50–200, and 80–300 at the initial, middle, and final stages, respectively, during 21 test runs of a 210-ton LF refining process. An increasing trend of $L_{S,measured}$ with the proceeding of LF refining process is observed; however, $L^{[Al]-[O],IMCT}_{S,calculated}$ by the IMCT model is much greater than $L_{S,measured}$ at each LF refining stage. This finding means that the calculated $a_{O,[Al]-[O]}$ based on the [Al]–[O] equilibrium with assuming the Al_2O_3 activity as 1 to represent $a_{O,bath}$ cannot be applied correctly in the developed IMCT model.

2. *Comparison of calculated $L^{(Al_2O_3)-[O],IMCT}_{S,calculated}$ by IMCT model using $a_{O,(Al_2O_3)-[O]}$ of molten steel at slag–metal interface and measured $L_{S,measured}$*

The relationship between the calculated $L^{(Al_2O_3)-[O],IMCT}_{S,calculated}$ by the IMCT model using $a_{O,(Al_2O_3)-[O]}$ under the (Al_2O_3)–[O] equilibrium with replacing the Al_2O_3 activity $a_{Al_2O_3}$ by $N_{Al_2O_3}$ from IMCT[29–33] to

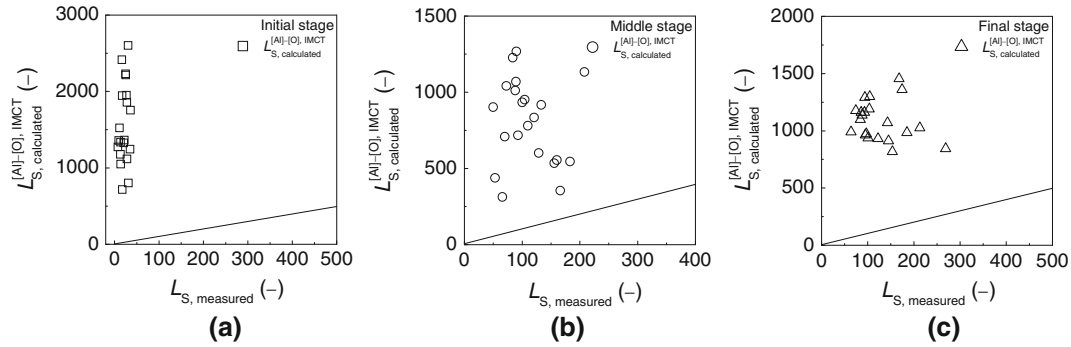

Fig. 8—Comparison of measured sulfur distribution ratio $L_{S,measured}$ and calculated sulfur distribution ratio $L_{S,calculated}^{[Al]-[O],IMCT}$ by the IMCT model with choosing $a_{Al_2O_3,s}$ under [Al]–[O] equilibrium by assuming $a_{Al_2O_3,s}$ as unity, *i.e.*, 1 to determine $a_{O,bath}$ at initial, middle, and final stages during 21 test runs of a 210-ton LF refining process, respectively.

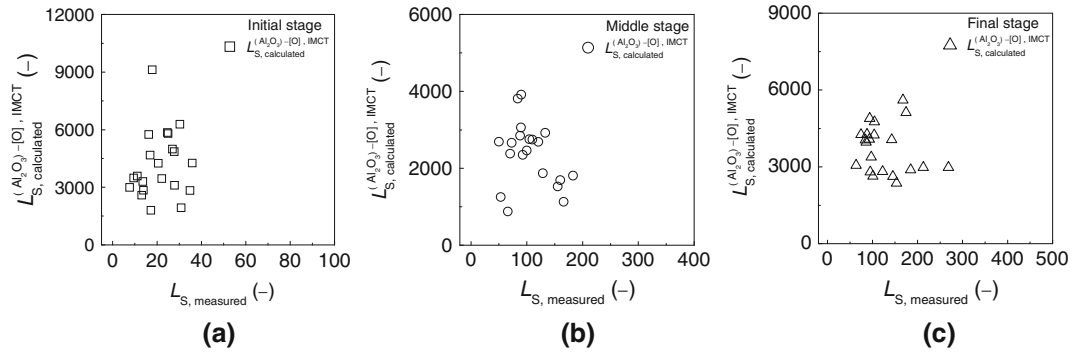

Fig. 9—Comparison of measured sulfur distribution ratio $L_{S,measured}$ and calculated sulfur distribution ratio $L_{S,calculated}^{(Al_2O_3)-[O],IMCT}$ by the IMCT model with choosing $a_{O,(Al_2O_3)-[O]}$ under (Al_2O_3)–[O] equilibrium by replacing Al_2O_3 activity $a_{Al_2O_3}$ by calculated mass action concentration of Al_2O_3 $N_{Al_2O_3}$ from IMCT to determine $a_{O,interface}$ at initial, middle, and final stages during 21 test runs of a 210-ton LF refining process, respectively.

represent $a_{O,interface}$ and the measured $L_{S,measured}$ at the initial, middle, and final stages during 21 test runs of a 210-ton LF refining process is shown in Figure 9, respectively. It can be observed from Figure 9 that the calculated $L_{S,calculated}^{(Al_2O_3)-[O],IMCT}$ by the IMCT model is much greater than $L_{S,measured}$ at three stages during the LF refining process. This result shows that the calculated $a_{O,(Al_2O_3)-[O]}$ based on the (Al_2O_3)–[O] equilibrium to represent the $a_{O,interface}$ cannot be reasonably applied in the developed IMCT model.

3. *Comparison of calculated $L_{S,calculated}^{(FeO)-[O],IMCT}$ by IMCT model using $a_{O,(FeO)-[O]}$ of molten steel at slag–metal interface and measured $L_{S,measured}$*

The relationship between the calculated $L_{S,calculated}^{(FeO)-[O],IMCT}$ by the IMCT model using $a_{O,(FeO)-[O]}$ under the (FeO)–[O] equilibrium with replacing the FeO activity a_{FeO} by N_{FeO} from IMCT[29–33] to represent $a_{O,(FeO)-[O]}^{interface}$ and the measured $L_{S,measured}$ at the initial, middle, and final stages during 21 test runs of a 210-ton LF refining process is shown in Figure 10, respectively. The calculated $L_{S,calculated}^{(FeO)-[O],IMCT}$ by the IMCT model is much greater than $L_{S,measured}$ at the initial stage; however, a good corresponding relationship between the calculated $L_{S,calculated}^{(FeO)-[O],IMCT}$ by the IMCT model and the measured $L_{S,measured}$ can be observed at both the middle and final stages during 21 test runs of LF refining process, although the relationship is to some degree scattered, respectively. This finding means that the calculated $a_{O,(Feo)-[O]}$ based on the (FeO)–[O] equilibrium with replacing the FeO activity a_{FeO} by N_{FeO} from IMCT[29–33] to represent $a_{O,interface}$ can be applied reasonably in the developed IMCT model at both the middle and final stages during 21 test runs of the LF refining process.

It can be obtained from Figure 10 and the related values of the measured $L_{S,measured}$ at the initial, middle, and final stages during 21 test runs of a 210-ton LF refining process listed in Tables I–III that the measured $L_{S,measured}$ in some test runs, such as in the No. 1, No. 2, No. 3, and No. 5 test runs, at the middle stage is greater than that at the final stage. However, the sulfur content shows a decreasing tendency from the initial stage in Table I to the final stage in Table III *via* the middle stage in Table II for the corresponding test runs, respectively. This conflicting result can be explained as follows: (a) the sulfur content in molten steel decreases with the proceeding of the LF refining process from the initial stage to the final stage *via* the middle stage because the desulfurization reactions in the LF refining reactor proceed with time prolonging; (b) some amount of the specially designed synthetic slags was added into

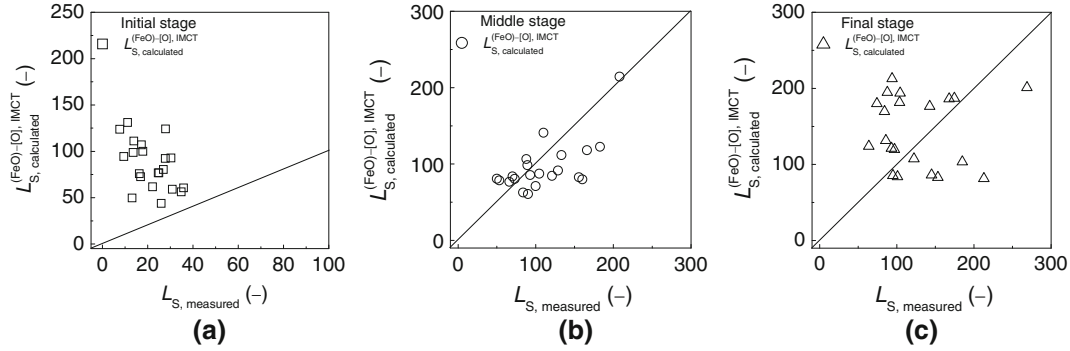

Fig. 10—Comparison of measured sulfur distribution ratio $L_{S,measured}$ and calculated sulfur distribution ratio $L_{S,calculated}^{(FeO)-[O],IMCT}$ by the IMCT model with choosing $a_{O,(FeO)-[O]}$ under (FeO)–[O] equilibrium by replacing FeO activity a_{FeO} by calculated mass action concentration of FeO N_{FeO} from IMCT to determine $a_{O,interface}$ at initial, middle, and final stages during 21 test runs of a 210-ton LF refining process, respectively.

the ladle after the middle stage if the analyzed sulfur content in molten steel cannot meet the requirement in the aimed steel as shown in Figure 1; and (c) the added specially designed synthetic slags can be verified from CaO content variation from the middle stage to the final stage for the related test runs, such as in No. 1, No. 2, No.3, and No. 5 test runs, because the CaO content in these test runs at the final stage in Table III is a little greater than that at the middle stage in Table II.

V. COMPARISON OF CALCULATED L_S BY THREE MODELS

To verify the feasibility of the developed IMCT model, it is necessary to compare the calculated $L_{S,calculated}^{IMCT}$ by the IMCT L_S prediction model with that by other L_S prediction models, such as Young's model[13] and the KTH model,[14–20] using three calculated oxygen activities, *i.e.*, $a_{O,[Al]-[O]}$, $a_{O,(Al_2O_3)-[O]}$, and $a_{O,(FeO)-[O]}$, to represent $a_{O,interface}$ at the desulfurization zone during the LF refining process.

A. *Young's Model*

The Young's L_S prediction model for predicting L_S is deduced from Young's model for predicting the sulfide capacity $C_{S^{2-}}$ model[13] combined with the relation[16,19,26] between $C_{S^{2-}}$ and L_S. The Young's model for predicting the $C_{S^{2}}$ of the slags can be summarized as follows:

$$\lg C_{S^{2-}} = -13.913 + 42.84\Lambda - 23.82\Lambda^2 - \frac{11710}{T} - 0.02223(\text{pct } SiO_2) - 0.02275(\text{pct } Al_2O_3) \quad (-)\,(\Lambda < 0.8) \qquad [31a]$$

$$C_{S^{2-}} = -0.6261 + 0.4808\Lambda + 0.7197\Lambda^2 + \frac{1697}{T} + \frac{2587\Lambda}{T} + 0.0005144(\text{pctFeO}) \quad (-)\,(\Lambda \geq 0.8) \qquad [31b]$$

The relationship between L_S and $C_{S^{2-}}$ can be formulated by considering the chemical composition of molten steel, such as a_O and f_S, as follows[16,19,26]

$$\lg L_S = \lg \frac{(\text{pct S})}{[\text{pct S}]} = -\frac{935}{T} + 1.375 + \lg C_{S^{2-}} + \lg f_S - \lg a_O \quad (-) \qquad [32]$$

Therefore, the Young's model[13] for predicting L_S of a slag equilibrated with metal is constituted by combining Eqs. [31] and [32].

B. *KTH Model*

Similar to Young's model[13] for predicting L_S, the KTH model for predicting L_S can be deduced from the KTH model[14–20] of predicting $C_{S^{2-}}$ combined with the relation[16,19,26] between $C_{S^{2-}}$ and L_S. The KTH model[14–20] for predicting $C_{S^{2-}}$ of the LF refining slags has been proposed as follows[20]:

$$\begin{aligned} RT(\ln C_{s^{2-}}) &= 58.8157T - 118535 \\ &\quad - (157705.28X_{Al_2O_3} - 33099.43X_{CaO} \\ &\quad + 9573.07X_{MgO} + 36626.46X_{MnO} + 168872.59X_{SiO_2}) \\ &\quad + \Big(\xi_{interaction}^{Al_2O_3-CaO} + \xi_{interaction}^{Al_2O_3-SiO_2} + \xi_{interaction}^{Al_2O_3-MnO} \\ &\quad + \xi_{interaction}^{CaO-SiO_2} + \xi_{interaction}^{MgO-SiO_2} + \xi_{interaction}^{MnO-SiO_2} + \xi_{interaction}^{CaO-FeO} \\ &\quad + \xi_{interaction}^{MnO-FeO} + \xi_{interaction}^{FeO-SiO_2} + \xi_{interaction}^{Al_2O_3-CaO-MgO} \\ &\quad + \xi_{interaction}^{Al_2O_3-CaO-SiO_2} + \xi_{interaction}^{Al_2O_3-MgO-SiO_2} + \xi_{interaction}^{Al_2O_3-MgO-MnO} \\ &\quad + \xi_{interaction}^{Al_2O_3-MnO-SiO_2} + \xi_{interaction}^{CaO-MgO-SiO_2} + \xi_{interaction}^{CaO-MnO-SiO_2} \\ &\quad + \xi_{interaction}^{MgO-MnO-SiO_2} + \xi_{interaction}^{Al_2O_3-FeO-SiO_2} + \xi_{interaction}^{CaO-FeO-SiO_2} \\ &\quad + \xi_{interaction}^{MgO-FeO-SiO_2} + \xi_{interaction}^{MnO-FeO-SiO_2}\Big) \end{aligned} \qquad [33]$$

where X_i is mole fraction of component i in slags (–) and $\xi_{interaction}^{i-j}$ is the defined interaction coefficient of component i to j in slags (–). The more detailed description

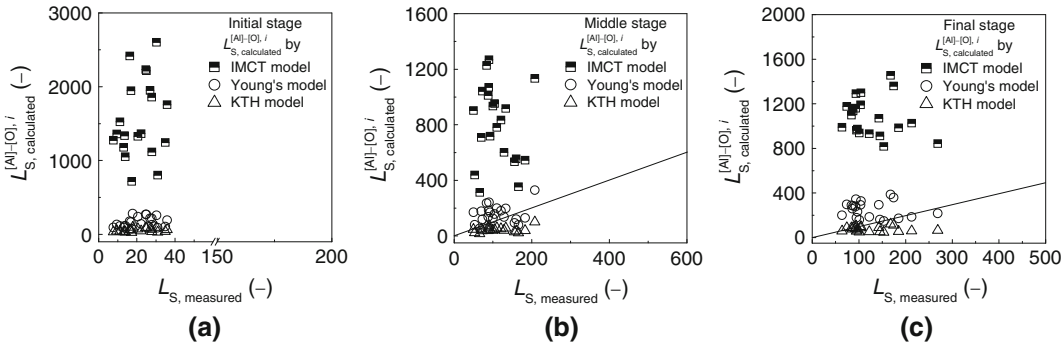

Fig. 11—Comparison of measured sulfur distribution ratio $L_{S,measured}$ and calculated sulfur distribution ratio $L_{S,calculated}^{[Al]-[O],i}$ by three L_S prediction models with choosing $a_{O,[Al]-[O]}$ under [Al]–[O] equilibrium by assuming $a_{Al_2O_3,s}$ as unity, *i.e.*, 1 to determine $a_{O,bath}$ at initial, middle, and final stages during 21 test runs of a 210-ton LF refining process, respectively.

of Eq. [33] and values of the related parameters in Eq. [33] have been described in detail elsewhere.[15,20] The KTH model for predicting L_S is composed by combining Eqs. [33] and [32].

C. *Results of Calculated $L_{S,calculated}^{i}$ by Three Models*

The different L_S prediction models have their limitations and application scope. Young's model is related with optical basicity Λ, temperature T, and the related component as shown in Eqs. [31] and [32], whereas the KTH model seriously depends on the defined interaction coefficient of component i to component j in the slags $\xi_{interaction}^{i-j}$, temperature T, and related components. All the related coefficients in Young's model and the KTH model are from a mathematical regression based on experimental data as empirical parameters with limited application scopes. Certainly, these coefficients in Young's model and the KTH model have no obvious metallurgical physicochemistry meaning. Young's model and the KTH model have been evaluated briefly elsewhere.[69]

The oxygen activity of molten steel a_O has an important effect or contribution on $L_{S,calculated}^{i}$ by the developed IMCT model, Young's model,[13] and the KTH model[14–20] simultaneously as shown in Eq. [32]. Therefore, to verify the optimal L_S prediction model among the three models, it is necessary to compare the measured $L_{S,measured}$ and the calculated $L_{S,calculated}^{i}$ by the previously mentioned three models using the different oxygen activities described in Section IV–B.

1. *Comparison of calculated $L_{S,calculated}^{[Al]-[O],i}$ by three L_S prediction models using $a_{O,[Al]-[O]}$ of bulk molten steel and measured $L_{S,measured}$*

The relationship between the measured $L_{S,measured}$ and the calculated $L_{S,calculated}^{[Al]-[O],i}$ by three models using $a_{O,[Al]-[O]}$ under the [Al]–[O] equilibrium with assuming $a_{Al_2O_3,s}$ as 1 to represent $a_{O,bath}$ at the initial, middle, and final stages during 21 test runs of the LF refining process is shown in Figure 11, respectively. At the initial stage, all $L_{S,calculated}^{[Al]-[O],i}$ by three L_S models are much larger than the measured $L_{S,measured}$; $L_{S,calculated}^{[Al]-[O],IMCT}$ by the IMCT model is the largest one compared with $L_{S,calculated}^{[Al]-[O],Young}$ by Young's model[13] and $L_{S,calculated}^{[Al]-[O],KTH}$ by the KTH model[14–20]; $L_{S,calculated}^{[Al]-[O],Young}$ by Young's model[13] is also greater than the measured $L_{S,measured}$; $L_{S,calculated}^{[Al]-[O],KTH}$ by the KTH model[14–20] is the smallest one compared with $L_{S,calculated}^{[Al]-[O],IMCT}$ by the IMCT model as well as $L_{S,calculated}^{[Al]-[O],Young}$ by Young's model,[13] but $L_{S,calculated}^{[Al]-[O],KTH}$ by the KTH model[14–20] is approximately two times greater than the measured $L_{S,measured}$. At the middle and final stages, $L_{S,calculated}^{[Al]-[O],IMCT}$ by the IMCT model is much larger than the measured $L_{S,measured}$; however, $L_{S,calculated}^{[Al]-[O],Young}$ by the Young's model[13] is also larger than the measured $L_{S,measured}$. $L_{S,calculated}^{[Al]-[O],KTH}$ by the KTH model is to some degree lower than the measured $L_{S,measured}$. Therefore, the previously mentioned three models cannot be reasonably used to predict the measured $L_{S,measured}$ by choosing $a_{O,[Al]-[O]}$ based on [Al]–[O] equilibrium with assuming $a_{Al_2O_3}$ as 1 to represent $a_{O,bath}$.

2. *Comparison of calculated $L_{S,calculated}^{(Al_2O_3)-[O],i}$ by three models using $a_{O,(Al_2O_3)-[O]}$ of molten steel at slag–metal interface and measured $L_{S,measured}$*

The relationship between the measured $L_{S,measured}$ and the calculated $L_{S,calculated}^{(Al_2O_3)-[O],i}$ by three models by choosing $a_{O,(Al_2O_3)-[O]}$ under (Al_2O_3)–[O] equilibrium with replacing the Al_2O_3 activity $a_{Al_2O_3}$ by $N_{Al_2O_3}$ from the IMCT[29–33] to represent $a_{O,interface}$ of the molten steel at the slag–metal interface at the initial, middle, and final stages during 21 test runs of the LF refining process is shown in Figure 12, respectively. The calculated $L_{S,calculated}^{(Al_2O_3)-[O],i}$ by three models is much greater than $L_{S,measured}$ at three stages during the LF refining process. The decreasing order of $L_{S,calculated}^{(Al_2O_3)-[O],i}$ by three models is $L_{S,calculated}^{(Al_2O_3)-[O],IMCT}$ by the IMCT model, then $L_{S,calculated}^{(Al_2O_3)-[O],Young}$ by Young's model,[13] and $L_{S,calculated}^{(Al_2O_3)-[O],KTH}$ by the KTH model.[14–20] It can be concluded that choosing $a_{O,(Al_2O_3)-[O]}$ under (Al_2O_3)–[O] equilibrium by replacing the Al_2O_3 activity $a_{Al_2O_3}$ by

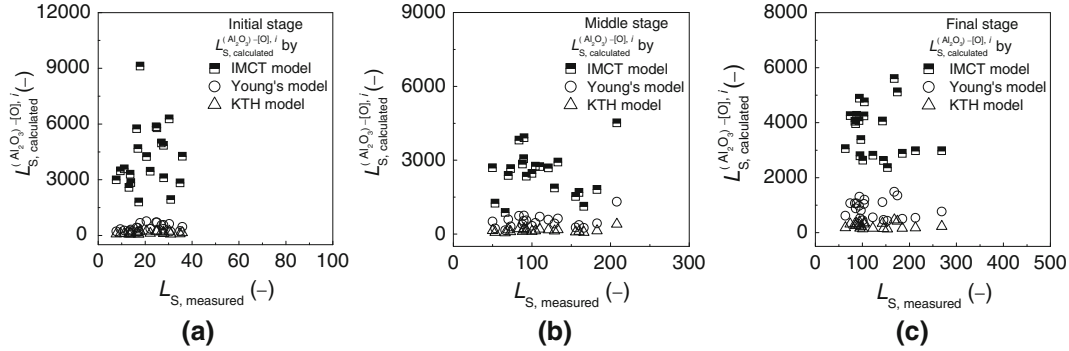

Fig. 12—Comparison of measured sulfur distribution ratio $L_{S,measured}$ and calculated sulfur distribution ratio $L_{S,calculated}^{(Al_2O_3)-[O],i}$ by three L_S prediction models with choosing $a_{O,(Al_2O_3)-[O]}$ under (Al_2O_3)–[O] equilibrium by replacing Al_2O_3 activity $a_{Al_2O_3}$ by calculated mass action concentration of Al_2O_3 $N_{Al_2O_3}$ from IMCT to determine $a_{O,interface}$ at initial, middle, and final stages during 21 test runs of a 210-ton LF refining process, respectively.

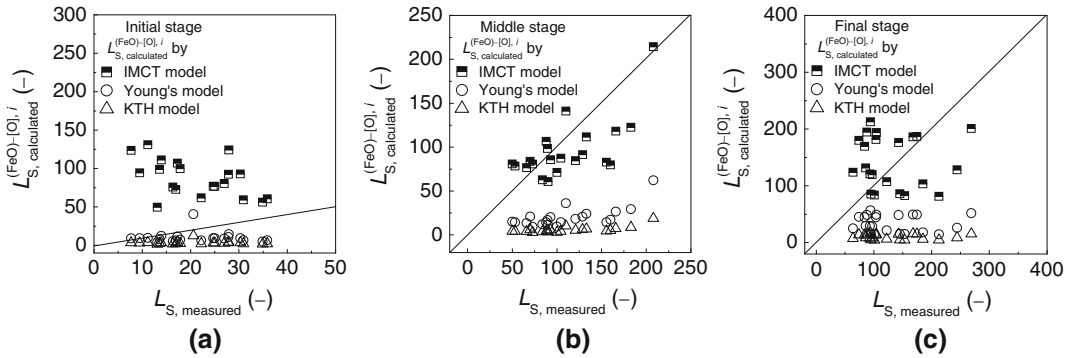

Fig. 13—Comparison of measured $L_{S,measured}$ and calculated $L_{S,calculated}^{(FeO)-[O],i}$ by three L_S prediction models by choosing $a_{O,(FeO)-[O]}$ under (FeO)–[O] equilibrium by replacing FeO activity a_{FeO} by calculated mass action concentration of FeO N_{FeO} from IMCT to determine $a_{O,interface}$ at initial, middle, and final stages during 21 test runs of a 210-ton LF refining process, respectively.

$N_{Al_2O_3}$ from the IMCT[29–33] to represent $a_{O,measured}$ cannot be applied in the three models during the LF refining process.

3. *Comparison of calculated $L_{S,calculated}^{(FeO)-[O],i}$ by three models using $a_{O,(FeO)-[O]}$ of molten steel at slag–metal interface and measured $L_{S,measured}$*

The relationship between the measured $L_{S,measured}$ and the calculated $L_{S,calculated}^{(FeO)-[O],i}$ by three models by choosing $a_{O,(FeO)-[O]}$ based on (FeO)–[O] equilibrium with replacing the FeO activity a_{FeO} by the N_{FeO} from IMCT[29–33] to represent $a_{O,interface}$ of molten steel at the slag–metal interface at the initial, middle, and final stages during 21 test runs of the LF refining process is shown in Figure 13, respectively. At the initial stage, $L_{S,calculated}^{(FeO)-[O],IMCT}$ by the IMCT model has no obvious relation with the measured $L_{S,measured}$; meanwhile, $L_{S,calculated}^{(FeO)-[O],IMCT}$ by the IMCT model is much greater than $L_{S,measured}$. However, $L_{S,calculated}^{(FeO)-[O],Young}$ by Young's model[13] and $L_{S,calculated}^{(FeO)-[O],KTH}$ by the KTH model is lower than $L_{S,measured}$. At the middle and final stages, $L_{S,calculated}^{(FeO)-[O],IMCT}$ by the IMCT model shows a clear corresponding relationship with the measured $L_{S,measured}$, although the linear relation is to some degree scattered. $L_{S,calculated}^{(FeO)-[O],Young}$ by Young's model[13] as well as $L_{S,calculated}^{(FeO)-[O],KTH}$ by the KTH model[14–20] is lower than $L_{S,measured}$, respectively. Therefore, only the developed IMCT model, rather than Young's model and the KTH model, can be reliably used to predict $L_{S,measured}$ by choosing $a_{O,(FeO)-[O]}$ under (FeO)–[O] equilibrium with replacing the FeO activity a_{FeO} by computed N_{FeO} from the IMCT to represent $a_{O,interface}$ at the middle and final stages during the LF refining process.

VI. CONTRIBUTION OF FREE BASIC OXIDES TO DESULFURIZATION ABILITY OF LF REFINING SLAGS

A. *Respective Sulfur Distribution Ratio of Free Basic Oxides in LF Refining Slags*

It was mentioned in Section IV–A that the total desulfurization ability of CaO–SiO_2–MgO–FeO–MnO–Al_2O_3 slags is composed of the respective desulfurization potential of its free basic oxides CaO, MgO, FeO, and MnO or ion couples $(Ca^{2+}+O^{2-})$, $(Mg^{2+}+O^{2-})$,

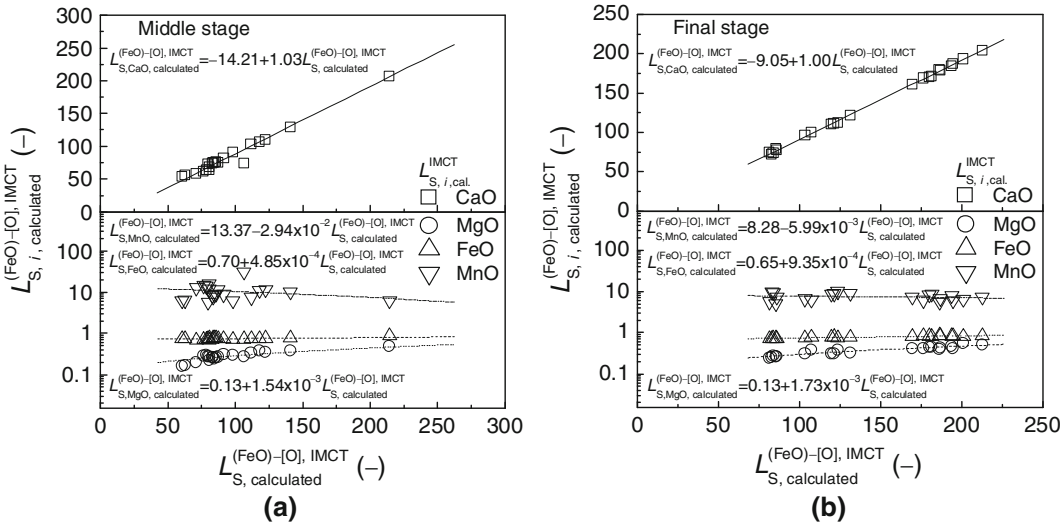

Fig. 14—Plot of calculated respective sulfur distribution ratio $L_{S,i,\text{calculated}}^{(FeO)-[O],IMCT}$ of ion couples $(Ca^{2+}+O^{2-})$, $(Mg^{2+}+O^{2-})$, $(Fe^{2+}+O^{2-})$, and $(Mn^{2+}+O^{2-})$ against calculated total sulfur distribution ratio $L_{S,\text{calculated}}^{(FeO)-[O],IMCT}$ of the slags by IMCT model at middle and final stages during 21 test runs of a 210-ton LF refining process, respectively.

$(Fe^{2+}+O^{2-})$, and $(Mn^{2+}+O^{2-})$ in the slags. To keep the consistency with the classically metallurgical physicochemistry, in which basic oxides in slags have desulfurization ability, the generated ion couples from these basic oxides have the same meaning with the corresponded free basic oxides in this study, such as ion couple $(Ca^{2+}+O^{2-})$ has the same meaning with free CaO.

The relationship between the calculated total sulfur distribution ratio $L_{S,\text{calculated}}^{(FeO)-[O],IMCT}$ of the slags and the respective sulfur distribution ratio $L_{S,i,\text{calculated}}^{(FeO)-[O],IMCT}$ of ion couples $(Ca^{2+}+O^{2-})$, $(Mg^{2+}+O^{2-})$, $(Fe^{2+}+O^{2-})$, and $(Mn^{2+}+O^{2-})$ in the slags by the developed IMCT model under the condition of choosing $a_{O,(FeO)-[O]}$ to represent the $a_{O,\text{interface}}$ of molten steel at the slag–metal interface as described in Section IV–B–3, Section IV–C–3 and Section V–C–3 at the middle and final stages during 21 test runs of the LF refining process is illustrated in Figure 14, respectively. A clear linear relation between $L_{S,\text{calculated}}^{(FeO)-[O],IMCT}$ and $L_{S,CaO,\text{calculated}}^{(FeO)-[O],IMCT}$ of ion couples $(Ca^{2+}+O^{2-})$ in the slags can be observed at both the middle and final stages with a slope of approximately 1.0. This finding implies that the desulfurization ability of the LF refining slags is mostly controlled by ion couple $(Ca^{2+}+O^{2-})$ in the slags. However, $L_{S,i,\text{calculated}}^{(FeO)-[O],IMCT}$ of the ion couples $(Mg^{2+}+O^{2-})$, $(Fe^{2+}+O^{2-})$, and $(Mn^{2+}+O^{2-})$ maintains almost constant values with the increasing $L_{S,\text{calculated}}^{(FeO)-[O],IMCT}$ of the slags as their slopes are small at both the middle and final stages during the LF refining process. Therefore, the intercepts of linear relations between $L_{S,\text{calculated}}^{(FeO)-[O],IMCT}$ of the slags and $L_{S,i,\text{calculated}}^{(FeO)-[O],IMCT}$ of ion couples $(Mg^{2+}+O^{2-})$, $(Fe^{2+}+O^{2-})$, and $(Mn^{2+}+O^{2-})$ can be considered as their contributions to the desulfurization ability of the slags. The decreasing order of desulfurization ability of ion couples in the slags at both the middle and final stages during the LF refining process is $(Ca^{2+}+O^{2-}) > (Mn^{2+}+O^{2-}) > (Fe^{2+}+O^{2-}) > (Mg^{2+}+O^{2-})$.

B. *Contribution Ratio of Free Basic Oxides to Calculated Sulfur Distribution Ratio of LF Refining Slags*

The relationship between the calculated total sulfur distribution ratio $L_{S,\text{calculated}}^{(FeO)-[O],IMCT}$ by the IMCT model by choosing $a_{O,(FeO)-[O]}$ to represent $a_{O,\text{interface}}$ of molten steel at the slag–metal interface as described in Section IV–B–3, Section IV–C–3, Section V–C–3, and Section VI–A, and the contribution ratio of the respective ion couples $(Ca^{2+}+O^{2-})$, $(Mg^{2+}+O^{2-})$, $(Fe^{2+}+O^{2-})$, and $(Mn^{2+}+O^{2-})$ in the slags to $L_{S,\text{calculated}}^{(FeO)-[O],IMCT}$ of the slag, *i.e.*, the ratio of $L_{S,i,\text{calculated}}^{(FeO)-[O],IMCT}$ to $L_{S,\text{calculated}}^{(FeO)-[O],IMCT}$, at both the middle and final stages during 21 test runs of the LF refining process is given in Figure 15, respectively. The average contribution ratio of the ion couple $(Ca^{2+}+O^{2-})$, $(Mn^{2+}+O^{2-})$, $(Fe^{2+}+O^{2-})$, and $(Mg^{2+}+O^{2-})$ in the slags to the calculated total sulfur distribution ratio of the slags is approximately 87–93 pct, 11.43–5.85 pct, 0.81–0.60 pct, and 0.30–0.27 pct at both the middle and final stages during 21 test runs of the LF refining process, respectively. This result suggests that ion couples both of $(Ca^{2+}+O^{2-})$ and $(Mn^{2+}+O^{2-})$ in the slags account for approximately 99 pct contribution, whereas the ion couples both of $(Mg^{2+}+O^{2-})$ and $(Fe^{2+}+O^{2-})$ in the slags have only approximately 1.0 pct contribution to $L_{S,\text{calculated}}^{(FeO)-[O],IMCT}$ at both the middle and final stages during the LF refining process.

C. *Contribution Ratio of Free Basic Oxides to Measured $L_{S,measured}$*

Considering the contribution ratio $L_{S,i,\text{calculated}}^{(FeO)-[O],IMCT}$ of the ion couples $(Ca^{2+}+O^{2-})$, $(Mg^{2+}+O^{2-})$,

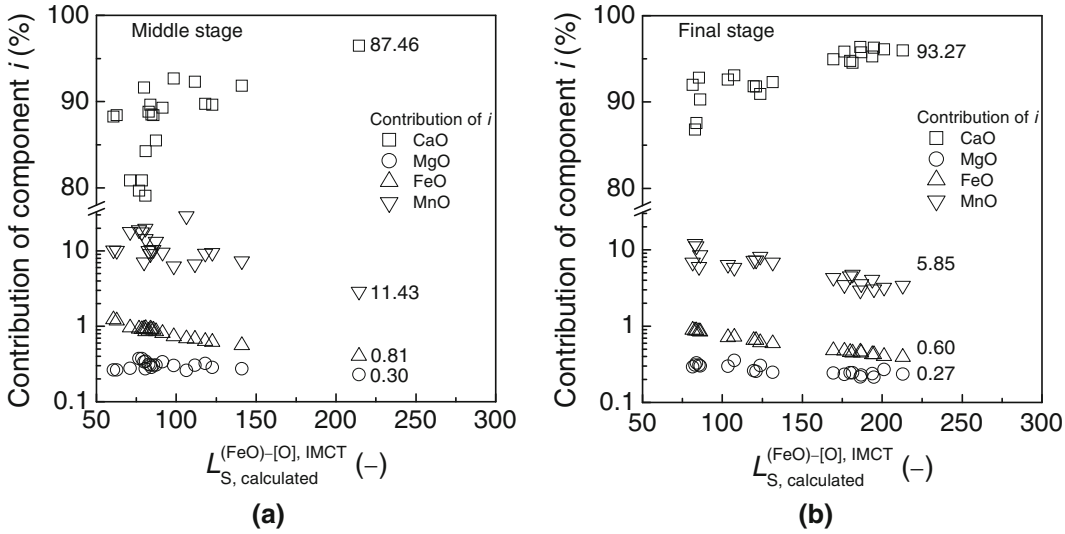

Fig. 15—Contribution ratio of ion couples $(Ca^{2+}+O^{2-})$, $(Mg^{2+}+O^{2-})$, $(Fe^{2+}+O^{2-})$, and $(Mn^{2+}+O^{2-})$ on calculated total sulfur distribution ratio $L^{(FeO)-[O],IMCT}_{S,calculated}$ of the slags by IMCT model at middle and final stages during 21 test runs of a 210-ton LF refining process, respectively.

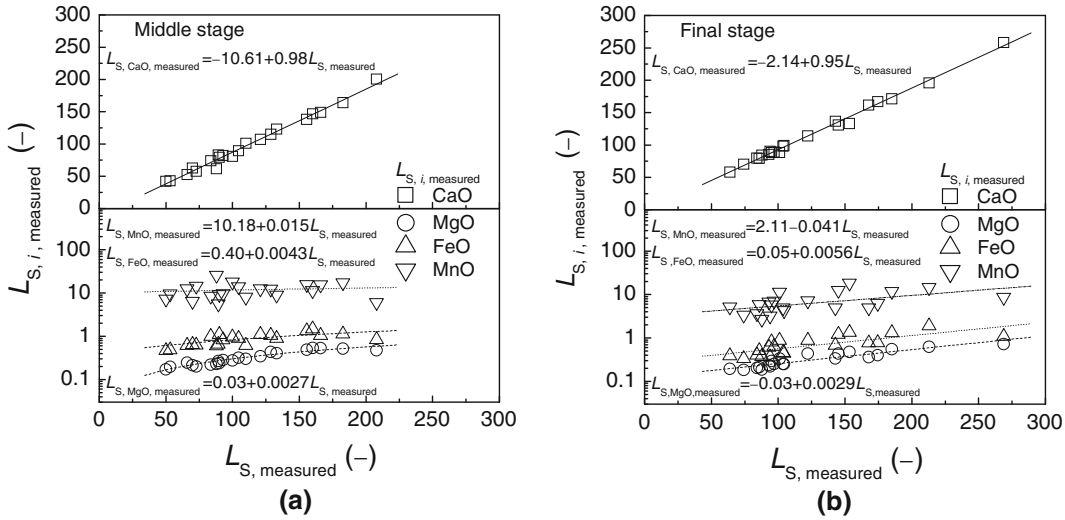

Fig. 16—Plot of calculated respective sulfur distribution ratio of ion couples $(Ca^{2+}+O^{2-})$, $(Mg^{2+}+O^{2-})$, $(Fe^{2+}+O^{2-})$, and $(Mn^{2+}+O^{2-})$ $L_{S,i,measured}$ against measured total sulfur distribution ratio $L_{S,measured}$ of the slags at middle and final stages during 21 test runs of a 210-ton LF refining process, respectively.

$(Fe^{2+}+O^{2-})$, and $(Mn^{2+}+O^{2-})$ in the slags to $L^{(FeO)-[O],IMCT}_{S,calculated}$ of the slags is the same as that to the measured $L_{S,measured}$. The respective sulfur distribution ratio $L_{S,i,measured}$ of the ion couple $(Ca^{2+}+O^{2-})$, $(Mg^{2+}+O^{2-})$, $(Fe^{2+}+O^{2-})$, and $(Mn^{2+}+O^{2-})$ can be also calculated from the developed IMCT model based on IMCT.[29–33] The relationship between the measured $L_{S,measured}$ and the calculated respective sulfur distribution ratio $L_{S,i,measured}$ of the ion couple $(Ca^{2+}+O^{2-})$, $(Mg^{2+}+O^{2-})$, $(Fe^{2+}+O^{2-})$, and $(Mn^{2+}+O^{2-})$ in the slags at both the middle and final stages during 21 test runs of LF refining process is illustrated in Figure 16, respectively. Similar to Figure 14, the slope of linear relation between the calculated $L_{S,CaO,measured}$ of ion couple $(Ca^{2+}+O^{2-})$ and the measured $L_{S,measured}$ is approximately 0.98 and 0.95 at both the middle and final stages during 21 test runs of the LF refining process, respectively. This finding implies that the ion couple $(Ca^{2+}+O^{2-})$ can control the desulfurization ability of the LF refining slags at both the middle and final stages during the LF refining process. No distinct change of the calculated respective sulfur distribution ratio $L_{S,i,measured}$ of the ion couples $(Mg^{2+}+O^{2-})$, $(Fe^{2+}+O^{2-})$, and $(Mn^{2+}+O^{2-})$ can be observed with an increase of the measured $L_{S,measured}$ because the slopes of the regressed linear relations are small. Under these circumstances, the intercepts of the regressed linear relationship between the calculated respective sulfur distribution ratio $L_{S,i,measured}$ of the ion couples $(Mg^{2+}+O^{2-})$, $(Fe^{2+}+O^{2-})$, and $(Mn^{2+}+O^{2-})$ in the slags and the measured $L_{S,measured}$ of the slags can be recommended to represent their respective contribution ratio.

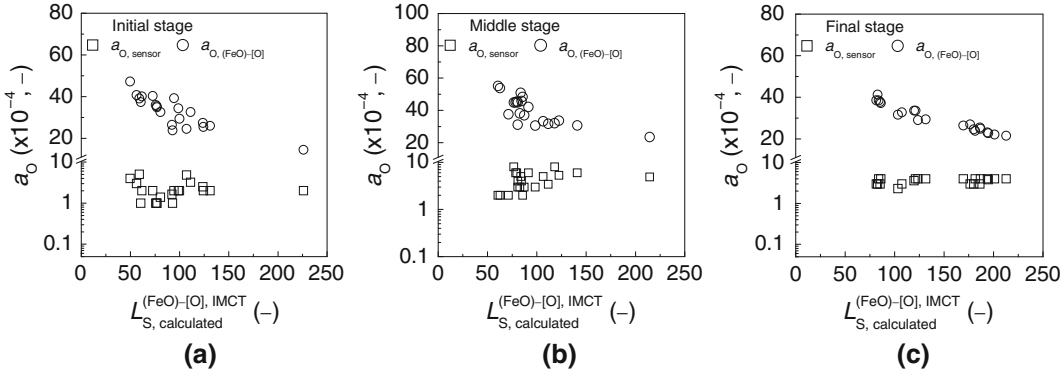

Fig. 17—Relationship between measured oxygen activity $a_{O,sensor}$ by the oxygen sensor or calculated oxygen activity $a_{O,(FeO)-[O]}$ under (FeO)–[O] equilibrium and calculated total sulfur distribution ratio $L_{S,calculated}^{(FeO)-[O],IMCT}$ of the slags by IMCT model at initial, middle, and final stages during 21 test runs of a 210-ton LF refining process, respectively.

VII. DESULFURIZATION MECHANISM DURING LF REFINING PROCESS

A. *Relation between Measured or Calculated Oxygen Activity of Molten Steel at Slag–Metal Interface and Calculated $L_{S,calculated}^{IMCT}$ by IMCT Model*

The relationship between the calculated $L_{S,calculated}^{(FeO)-[O],IMCT}$ by the IMCT model by choosing $a_{O,(FeO)-[O]}$ to represent the $a_{O,interface}$ of the molten steel at the slag–metal interface and the measured $a_{O,sensor}$ of the bulk molten steel by the oxygen sensor or the calculated $a_{O,(FeO)-[O]}$ based on (FeO)–[O] equilibrium with replacing the FeO activity a_{FeO} by N_{FeO} from IMCT[29–33] at the initial, middle, and final stages during 21 test runs of the LF refining process is illustrated in Figure 17, respectively. The measured $a_{O,sensor}$ of bulk molten steel by the oxygen sensor, which is basically equal to the calculated $a_{O,[Al]-[O]}$ under [Al]–[O] equilibrium with assuming the Al_2O_3 activity $a_{Al_2O_3,s}$ as 1, maintains a small value as 10×10^{-4} during the entire LF refining process. This finding suggests that the chemical composition of molten steel, including dissolved oxygen [O], is uniform with an ideal stirring by bottom blowing Ar gas. However, the desulfurization reactions of molten steel during the LF refining process are carried out through the slag–metal interface by contacting the slags and molten steel as shown in Eq. [16]. The calculated $a_{O,(FeO)-[O]}$ of molten steel at the slag–metal interface is more important than the measured $a_{O,sensor}$ of bulk molten steel by the oxygen sensor. The calculated $a_{O,(FeO)-[O]}$ of molten steel at the slag–metal interface under (FeO)–[O] equilibrium in a range of 20×10^{-4} through 50×10^{-4} is much greater than the measured $a_{O,sensor}$ in a range of 2×10^{-4} through 4×10^{-4}, and it shows an obvious decreasing tendency with an increase of the calculated $L_{S,calculated}^{(FeO)-[O],IMCT}$ by the IMCT model at the initial, middle, and final stages during the LF refining process. The result of lower oxygen activity $a_{O,(FeO)-[O]}$ corresponding to greater L_S can be clearly explained by L_S formula of IMCT. It is a distinct proof to show the feasibility of the developed IMCT model.

Therefore, it can be concluded that the desulfurization process during the LF refining process of refining pipeline steel is not controlled by the desulfurization reactions but is governed by oxygen diffusion from molten steel at the slag–metal interface to bulk molten steel. Enhancing the stirring of molten steel beneath the slag–metal interface is a promising measure to strengthen the desulfurization reactions or shorten the refining period compared with the modifying of bottom blowing Ar gas operation during LF refining process.

B. *Relation between Measured or Calculated Oxygen Activity of Molten Steel at Slag–Metal Interface and Measured $L_{S,measured}$*

Because the linear relation between the measured $L_{S,measured}$ and the calculated $L_{S,calculated}^{(FeO)-[O],IMCT}$ by the IMCT model by taking $a_{O,(FeO)-[O]}$ to represent $a_{O,interface}$ of molten steel at the slag–metal interface is scattered to some degree at the middle and final stages during 21 test runs of the LF refining process as shown in Figure 13(b) and (c), it is necessary to compare the effects of both the measured $a_{O,sensor}$ of bulk molten steel by the oxygen sensor and the calculated $a_{O,(FeO)-[O]}$ of molten steel at the slag–metal interface on the measured $L_{S,measured}$. The relationship between the measured $L_{S,measured}$ and the measured $a_{O,sensor}$ of the bulk molten steel by the oxygen sensor or the calculated $a_{O,(FeO)-[O]}$ under (FeO)–[O] equilibrium at the initial, middle, and final stages during 21 test runs of the LF refining process is illustrated in Figure 18, respectively. The calculated $a_{O,(FeO)-[O]}$ based on (FeO)–[O] equilibrium at the initial stage is larger than the measured $a_{O,sensor}$ of the bulk molten steel as shown in Figure 18(a), but no clear corresponding relation between the calculated $a_{O,(FeO)-[O]}$ based on (FeO)–[O] equilibrium and the measured $L_{S,measured}$ can be observed at the initial stage. The measured $L_{S,measured}$ and the calculated $L_{S,calculated}^{(FeO)-[O],IMCT}$ by the IMCT model by choosing $a_{O,(FeO)-[O]}$ to represent $a_{O,interface}$ has no corresponding relation at the initial stage as shown in Figure 13(a) because the desulfurization

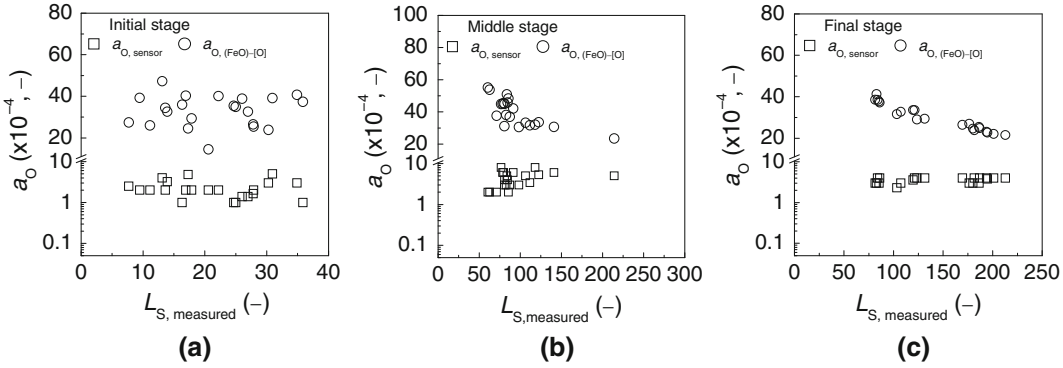

Fig. 18—Relationship between measured oxygen activity $a_{O,sensor}$ by the oxygen sensor or calculated oxygen activity $a_{O,(FeO)–[O]}$ under (FeO)–[O] equilibrium and measured total sulfur distribution ratio $L_{S,measured}$ of the slags at initial, middle, and final stages during 21 test runs of a 210-ton LF refining process, respectively.

reactions at the initial stage are far from the thermodynamic equilibrium during the LF refining process. As a basis, plotting Figure 18(a) is just for a convenient comparison with that at the middle and final stages, respectively. The results shown in Figures 18(b) and (c) are similar as that in Figures 17(b) and (c), *i.e.*, the smaller the calculated $a_{O,(FeO)–[O]}$ of molten steel at the slag–metal interface under (FeO)–[O] equilibrium, the larger the measured $L_{S,measured}$ of the LF refining slags. It is verified that decreasing the $a_{O,(FeO)–[O]}$ of molten steel at the slag–metal interface is more beneficial to enhance the desulfurization than decreasing the $a_{O,sensor}$ of bulk molten steel during the LF refining process because the measured $a_{O,sensor}$ by the oxygen sensor is small enough at 2×10^{-4} through 4×10^{-4}.

Therefore, the desulfurization mechanism between the LF refining slags and molten steel during the LF refining process can be schematically illustrated in Figure 19 from the previously mentioned discussion and results. The result that existing a high-oxygen-activity boundary layer beneath the slag–metal interface during the LF refining process is not conflict or opposite to that of the higher oxygen activity at a lower measurement position in ladle reported by Björklund *et al.*[70] because the proposed high-oxygen-activity boundary layer beneath slag–metal interface will be very thin.

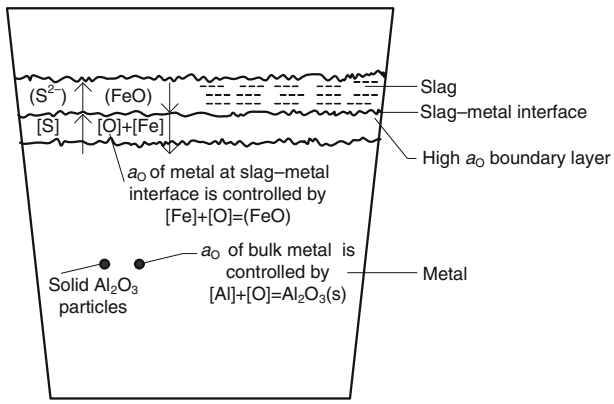

Fig. 19—Schematic illustration of desulfurization reaction mechanism during the LF refining process based on oxygen potential gradient of molten steel at slag–metal interface and of bulk molten steel.

VIII. CONCLUSIONS

A thermodynamic model for calculating the sulfur distribution ratio between the LF refining slags and molten steel has been developed by coupling with a developed thermodynamic model for calculating the mass action concentrations of structural units or ion couples in $CaO–SiO_2–MgO–FeO–MnO–Al_2O_3$ LF refining slags based on the IMCT. The calculated sulfur distribution ratio between the LF refining slags and molten steel by the developed IMCT sulfur distribution ratio prediction model has been verified with the measured and calculated by Young's model and the KTH model at the initial, middle, and final stages in a 210-ton LF refining reactor for refining pipeline steel. The main summary remarks are as follows:

1. The calculated equilibrium mole numbers or mass action concentrations of the structural units or ion couples, rather than mass percentage of components, are recommended to represent the reaction ability of components in $CaO–SiO_2–MgO–FeO–MnO–Al_2O_3$ slags equilibrated or reacted with molten steel during the LF process of refining the pipeline steel.
2. Increasing (pct CaO) from 49 pct to 58 pct, decreasing (pct Al_2O_3) from 33 pct to 26 pct, and maintaining (pct MgO) constant as 9–10 pct can lead to maintaining the equilibrium mole number of ion couple $(Mg^{2+} + O^{2-})$ as constant as 0.4 mol and increasing the total equilibrium mole number of all structural units from 1.435 mol to 1.633 mol in $CaO–SiO_2–MgO–FeO–MnO–Al_2O_3$ slags at both the middle and final stages during the LF refining process.
3. Not only the total sulfur distribution ratio between the LF refining slags and molten steel but also the respective sulfur distribution ratio between the four basic oxides in the LF refining slags and molten steel can be predicted by the developed IMCT sulfur distribution ratio prediction model. Choosing the oxygen activity of molten steel at the slag–metal interface or in bulk molten steel has a crucial effect on the

predicted results of sulfur distribution ratio by the IMCT model.

4. The developed IMCT model can be reliably used to calculate the LF refining sulfur distribution ratio between the LF refining slags and molten steel by using the oxygen activity of molten steel at the slag–metal interface under (FeO)–[O] equilibrium.
5. The measured sulfur distribution ratio between the LF refining slags and molten steel can only be reliably predicted by the developed IMCT model, rather than other models such as Young's model and the KTH model.
6. Large differences of desulfurization ability are found among the free components of CaO, MgO, FeO, and MnO in $CaO–SiO_2–MgO–FeO–MnO–Al_2O_3$ slags during the LF refining process. The average contribution ratio of the ion couple $(Ca^{2+}+O^{2-})$, $(Mn^{2+}+O^{2-})$, $(Fe^{2+}+O^{2-})$, and $(Mg^{2+}+O^{2-})$ to the calculated sulfur distribution ratio is approximately 87–93 pct, 11.43–5.85 pct, 0.81–0.60 pct, and 0.30–0.27 pct at both the middle and final stages during the LF refining process, respectively.
7. A large gradient of oxygen potential or oxygen activity is found in the molten steel beneath the slag–metal interface and in bulk molten steel. The oxygen potential or oxygen activity of molten steel at the slag–metal interface is controlled by (FeO)–[O] equilibrium, whereas the oxygen activity in the bulk molten steel is controlled by [Al]–[O] equilibrium during the LF refining process for producing pipeline steel. The oxygen activity in molten steel at the slag–metal interface, rather than oxygen activity in bulk molten steel, affects the desulfurization reactions. Effectively reducing or destroying the high-oxygen-activity boundary layer beneath the slag–metal interface can largely promote the desulfurization reaction rate or shorten the refining period during the LF refining process.

ACKNOWLEDGMENTS

The authors sincerely appreciate Prof. Jian Zhang, who is a founder of the ion and molecule theory, for providing helpful discussions and encouragement. The sincere thanks are also extended to Prof. Chang–xiang Xiang, on metallurgical physicochemistry at the School of Metallurgical and Ecological Engineering, University of Science and Technology Beijing, for valuable discussion and helps for preparing Section III–B–4 on deciding the standard molar Gibbs free energy change of related reactions. Meanwhile, heartfelt thanks are also extended to Shougang Qian'an Iron and Steel Company Limited for carrying out the industrial experiments and permitting the authors to publish the related results.

NOMENCLATURE

A	constant, (–)
a_i	activity of component i in molten steel or slags, (–)
$a_{O,interface}$	oxygen activity of molten steel at slag–metal interface, (–)
$a_{O,bath}$	oxygen activity of bulk molten steel, (–)
$a_{O,sensor}$	measured oxygen activity in molten steel by oxygen sensor, (–)
$a_{O,[Al]–[O]}$	calculated oxygen activity of bulk molten steel based on [Al]–[O] equilibrium, (–)
$a_{O,(Al_2O_3)–[O]}$	calculated oxygen activity of molten steel at slag–metal interface based on (Al_2O_3)–[O] equilibrium, (–)
$a_{O,(FeO)–[O]}$	calculated oxygen activity of molten steel at slag–metal interface based on (FeO)–[O] equilibrium, (–)
$a_{O^{2-}}$	oxygen ion activity in slags, (–)
b_i	mole number of component i in 100-g slags, (mol)
B	constant, (–)
$C_{S^{2-}}$	sulfide capacity of the slags, (–)
e_i^j	activity interaction coefficient of component j on component i in molten steel based on mass percentage as concentration unit and one mass percent (1 pct) as standard state, (–)
f_i	activity coefficient of component i in molten steel, (–)
$\Delta_r G^{\Theta}_{m,i}$	standard molar Gibbs free energy change of forming component i or structural unit i in slags, (J/mol)
$\Delta_r G^{\Theta}_{m,i(s)}$	standard molar Gibbs free energy change of forming component i as solid, (J/mol)
$\Delta_{fus} G^{\Theta}_{m,i}$	standard molar Gibbs free energy change of melting component i or structural unit i from solid to liquid, (J/mol)
$\Delta_{sol} G^{\Theta}_{m,i}$	standard molar Gibbs free energy change of dissolving component i or structural unit i into slags, (J/mol)
K_i^{Θ}	equilibrium constant of chemical reaction for forming component i or structural unit i, (–)
L_S	sulfur distribution ratio between slags and molten steel, (–)
$L_{S,i}$	calculated respective sulfur distribution ratio of free component i or ion couple i in slags, (–)
$L_{S,measured}$	measured sulfur distribution ratio, (–)
$L_{S,calculated}$	calculated total sulfur distribution ratio between slags and molten steel, (–)
$L_{S,i,\ measured}$	calculated respective sulfur distribution ratio of component i or ion couple i in slags from measured data, (–)
$L^{IMCT}_{S,calculated}$	calculated total sulfur distribution ratio between slags and molten steel by the IMCT model, (–)
$L^{[Al]–[O]}_{S,calculated}$	calculated total sulfur distribution ratio between slags and molten steel based on [Al]–[O] equilibrium for determining activity of oxygen at slag–metal interface $a_{O,interface}$, (–)

$L_{S,calculated}^{(Al_2O_3)-[O]}$ calculated total sulfur distribution ratio between slags and molten steel based on (Al_2O_3)–[O] equilibrium for determining activity of oxygen at slag–metal interface $a_{O,interface}$, (–)

$L_{S,calculated}^{(FeO)-[O]}$ calculated total sulfur distribution ratio between slags and molten steel based on (FeO)–[O] equilibrium for determining activity of oxygen at slag–metal interface $a_{O,interface}$, (–)

$L_{S,calculated}^{(FeO)-[O],IMCT}$ calculated total sulfur distribution ratio between slags and molten steel by the IMCT model based on (FeO)–[O] equilibrium for determining activity of oxygen at slag–metal interface $a_{O,interface}$, (–)

$L_{S,calculated}^{(FeO)-[O],Young}$ calculated total sulfur distribution ratio between slags and molten steel by Young's model based on (FeO)–[O] equilibrium for determining activity of oxygen at slag–metal interface $a_{O,interface}$, (–)

$L_{S,calculated}^{(FeO)-[O],KTH}$ calculated total sulfur distribution ratio between slags and molten steel by the KTH model based on (FeO)–[O] equilibrium for determining activity of oxygen at slag–metal interface $a_{O,interface}$, (–)

$L_{S,i,calculated}^{(FeO)-[O],IMCT}$ calculated respective sulfur distribution ratio of component i or ion couple i in slags by the IMCT model based on (FeO)–[O] equilibrium for determining activity of oxygen at slag–metal interface $a_{O,interface}$, (–)

Me metal, (–)

M_i molecular weight of element i or component i, (g/mol)

n_i^0 mole number of components i in 100-g slags, (mol)

n_i equilibrium mole number of structural unit i or ion couple i in 100-g slags based on IMCT, (mol)

N_i mass action concentrations of structural unit i or ion couple i in the slags based on IMCT, (–)

Σn_i total equilibrium mole number of all structural units in 100-g slags based on IMCT, (mol)

R gas constant, (8.314 J/(mol·K))

T absolute temperature, (K)

X_i mole fraction of component i in the slags, (–)

(pct i) mass percentage of component i in slags, (–)

[pct i] mass percentage of component i in molten steel, (–)

$(pct\ S)_{CaS}$ sulfur content in slags boned as CaS, (–)

$(pct\ S)_{MgS}$ sulfur content in slags boned as MgS, (–)

$(pct\ S)_{FeS}$ sulfur content in slags boned as FeS, (–)

$(pct\ S)_{MnS}$ sulfur content in slags boned as MnS, (–)

GREEK SYMBOLS

Λ optical basicity of slags (–)

$\xi_{interaction}^{i-j}$ interaction coefficient of component i to component j in slags defined in the KTH model, (–)

$\mu_{i(s)}^*$ chemical potential of component i as solid, (J/mol)

$\mu_{i(1)}^*$ chemical potential of component i as liquid, (J/mol)

μ_i^Θ standard chemical potential of dissolved component i in slags, (J/mol)

SUBSCRIPTS

ci complex molecule i, (–)

REFERENCES

1. D. Takahashi, M. Kamo, Y. Kurose, and H. Nomura: *Ironmaking Steelmaking*, 2003, vol. 30 (2), pp. 116–19.
2. J. Diao, B. Xie, and S.S. Wang: *Ironmaking Steelmaking*, 2009, vol. 36 (7), pp. 543–47.
3. P.K. Iwamasa and R.J. Fruehan: *Metall. Mater. Trans. B*, 1997, vol. 28B, pp. 47–57.
4. D.S. Vinoo, D. Mazumdar, and S.S. Gupta: *Ironmaking Steelmaking*, 2007, vol. 34 (6), pp. 471–76.
5. G. Yuasa, T. Yajima, A. Ukai, and M Ozawa: *Trans. ISIJ*, 1984, vol. 24 (5), pp. 412–18.
6. H.X. Tian, Z.Z. Mao, and Y. Wang: *ISIJ Int.*, 2008, vol. 48 (1), pp. 58–62.
7. H.X. Tian, Z.Z. Mao, and A.N. Wang: *ISIJ Int.*, 2009, vol. 49 (1), pp. 58–63.
8. A. Margareta, T. Andersson, L.T.I. Jonsson, and P.G. Jönsson: *Scand. J. Metall.*, 2003, vol. 32 (3), pp. 123–36.
9. M.A.T. Andersson, L.T.I. Jonsson, and P.G. Jönsson: *ISIJ Int.*, 2000, vol. 40 (11), pp. 1080–88.
10. F.D. Richardson and C.J.B. Fincham: *J. Iron Steel Inst.*, 1954, vol. 178 (9), pp. 4–15.
11. C.J.B. Fincham and F.D. Richardson: *Proc. Roy. Soc., London*, 1954, vol. 223A, pp. 40–62.
12. X.M. Yang, T.Z. Liu, Z.C. Guo, X.P. YU, and D.G. Wang: *J. Iron Steel Res.*, 1995, vol. 7 (6), pp. 1–8.
13. R.W. Young, J.A. Duffy, G.J. Hassall, and Z. Xu: *Ironmaking Steelmaking*, 1992, vol. 19 (3), pp. 201–19.
14. D. Sichen, R. Nilsson, and S. Seetharaman: *Steel Res.*, 1995, vol. 66 (11), pp. 458–62.
15. M.M. Nzotta, D. Sichen, and S. Seetharaman: *ISIJ Int.*, 1998, vol. 38 (11), pp. 1170–79.
16. M.A.T. Andersson, P.G. Jönsson, and M.M. Nzotta: *ISIJ Int.*, 1999, vol. 39 (11), pp. 1140–49.
17. M.M. Nzotta, D. Sichen, and S. Seetharaman: *ISIJ Int.*, 1999, vol. 39 (7), pp. 657–63.
18. M. Andersson: Ph.D. Dissertation, Royal Institute of Technology, Stockholm, Sweden, 2000.
19. M.A.T. Andersson, P.G. Jönsson, and M. Hallberg: *Ironmaking Steelmaking*, 2000, vol. 27 (4), pp. 286–92.
20. M.M. Nzotta, D. Sichen, and S. Seetharaman: *Metall. Mater. Trans. B*, 1999, vol. 30B, pp. 909–20.
21. D.J. Sosinsky and I.D. Sommerville: *Metall. Trans. B*, 1986, vol. 17B, pp. 331–37.
22. R.G. Reddy and M. Blander: *Metall. Trans. B*, 1987, vol. 18B, pp. 591–96.

23. M. Hino, S. Kitagawa, and S. Ban-ya: *ISIJ Int*., 1993, vol. 33 (1), pp. 36–42.
24. R. Nilsson, S. Seetharaman, and K.T. Jacob: *ISIJ Int*., 1994, vol. 34 (11), pp. 876–82.
25. S. Ban-ya, M. Hobo, T. Kaji, T. Itoh, and M. Hino: *ISIJ Int*., 2004, vol. 44 (11), pp. 1810–16.
26. A. Shankar: *Ironmaking Steelmaking*, 2006, vol. 33 (5), pp. 413–18.
27. A. Shankar, M. Gornerup, A.K. Lahiri, and S. Seetharaman: *Metall. Mater. Trans. B*, 2006, vol. 37B, pp. 941–47.
28. Y. Taniguchi, N. Sano, and S. Seetharaman: *ISIJ Int*., 2009, vol. 49 (2), pp. 156–63.
29. X.M. Yang, J.S. Jiao, R.C. Ding, C.B. Shi, and H.J. Guo: *ISIJ Int*., 2009, vol. 49 (12), pp. 1828–37.
30. J. Zhang: *Acta Metall. Sin. (English Lett.)*, 2001, vol. 14 (3), pp. 177–90.
31. J. Zhang: *J. Univ. Sci. Technol. Beijing*, 2002, vol. 9 (2), pp. 90–98.
32. J. Zhang: *Rare Metals*, 2004, vol. 23 (3), pp. 209–13.
33. J. Zhang: *Computational Thermodynamics of Metallurgical Melts and Solutions*, Metallurgical Industry Press, Beijing, China, 2007.
34. Verein Deutscher Eisenhüttenleute, *Slag Atlas*, 2nd ed., Woodhead Publishing Limited, Abington, Cambridge, UK, 1995.
35. E.T. Turkdogan: *Physical Chemistry of High Temperature Technology*, Academic Press Inc, New York, NY, 1980, pp. 8–12.
36. R.H. Rein and J. Chipman: *Trans. TMS-AIME*, 1965, vol. 233 (2), pp. 415–25.
37. H. Gaye and J. Welfringer: *Proc. 2nd Int Symp. Metalll Slags and Fluxes*, TMS-AIME, Lake Tahoe, NV, 1984, pp. 357–75.
38. K. Narita and K. Shinji: *Kobe Steel Engineering Reports*, 1969, vol. 19, pp. 25–42.
39. The Japan Society for the Promotion of Science: *The 19th Committee on Steelmaking: Steelmaking Data Sourcebook*, Gordon and Breach Science Publishers, New York, NY, 1988.
40. S. Ban-ya, A. Chiba, and A. Hirosaka: *Tetsu–to–Hagané*, 1980, vol. 66 (10), pp. 1484–93.
41. M. Timucin and A. Muan: *J. Am. Ceram. Soc*., 1992, vol. 75 (6), pp. 1399–406.
42. J. Zhang: *J. Beijing Univ. Iron Steel Technol*., 1986, vol. 8, pp. 1–6.
43. J. Zhang: *J. Beijing Univ. Iron Steel Technol*., 1988, vol. 10, pp. 1–6.
44. P. Wang, T.W. Ma, and J. Zhang: *Iron Steel*, 1996, vol. 31, pp. 27–31.
45. J. Zhang and C. Wang: *J. Univ. Sci. Technol. Beijing*, 1991, vol. 13, pp. 214–21.
46. J. Zhang and W.X. Yuan: *J. Univ. Sci. Technol. Beijing*, 1995, vol. 17, pp. 418–23.
47. J. Zhang: *Acta Metall. Sin*., 1998, vol. 34, pp. 742–52.
48. J. Zhang and P. Wang: *CALPHAD*, 2001, vol. 25, pp. 343–54.
49. H. Guo, Y.T. Hu, D.Q. Cang, Y. Jin, L.X. Wang, X.L. Cheng, H. Bai, and Y.B. Zong: *Chinese Chem. Lett*., 2010, vol. 21, pp. 229–33.
50. S.K. Wei: *Thermodynamics of Metallurgical Processes* (series book of modern metallurgy), Shanghai Scientific & Technical Publishers, Shanghai, China, 1980, pp. 52, 292, 396–98.
51. J.Y. Zhang: *Metallurgical Physicochemistry*, Metallurgical Industry Press, Beijing, China, 1980, p. 42.
52. R. Tsujino, J. Nakashima, M. Hirai, and Y. Yamada: *ISIJ Int*., 1989, vol. 29 (1), pp. 92–95.
53. M. Ohya: *Ferrous Metallurgy and Thermodynamics*, Nikkan Kogyo Shimbun–sha, Tokyo, Japan, 1971.
54. J. Yang, M. Kuwabara, K. Okumura, and M. Sano: *ISIJ Int*., 2005, vol. 45 (12), pp. 1795–803.
55. J. Lee and K. Morita: *ISIJ Int*., 2004, vol. 44 (2), pp. 235–42.
56. E.T. Turkdogan: *ISIJ Int*., 2000, vol. 40 (10), pp. 964–70.
57. G.K. Sigworth and J.F. Elliott: *Met. Sci*., 1974, vol. 8 (9), pp. 298–310.
58. J.F. Elliott, M. Gleiser, and V. Ramakrisha: *Thermochemistry for Steelmaking*, Addison–Wesley Publishing Co., London, UK, 1963, vol. 2, pp. 620–21.
59. H. Ohta and H. Suito: *Metall. Mater. Trans. B*, 1995, vol. 26B, pp. 295–303.
60. J. Tanabe, I, Seki, and K, Nagata: *ISIJ Int*., 2006, vol. 46 (2), pp. 169–73.
61. R. Tsujino, J. Nakashima, M. Hirai, and Y. Yamada: *ISIJ Int*., 1989, vol. 29 (1), pp. 92–95.
62. D.G.C. Robertson, B. Deo, and S. Ohguchi: *Ironmaking Steelmaking*, 1984, vol. 11 (1), pp. 41–53.
63. R. Markus and P. Wolfgang: *Steel Res*., 1994, vol. 65 (8), pp. 309–14.
64. H. Ohta and H. Suito: *Metall. Mater. Trans. B*, 1998, vol. 29B, pp. 119–29.
65. T. Tsao and H.G. Katayama: *ISIJ Int*., 1986, vol. 26 (8), pp. 717–23.
66. *The Recommended Values for the Equilibrium of Steelmaking Reactions,* ed.: The Japan Society for the Promotion of Science, Nikan Kogyo Shinbunsha, Tokyo, Japan, 1968.
67. D.B. Hyun and J.B. Shim: *ISIJ Int*., 1988, vol. 28 (9), pp. 736–45.
68. I.H. Jung, S.A. Decterov, and A.D. Pelton: *Metall. Mater. Trans. B*, 2004, vol. 35B, pp. 877–89.
69. C.B. Shi, X.M. Yang, J.S. Jiao, C. Li, and H.J. Guo: *ISIJ Int*., 2010, vol. 50 (10), pp. 1362–72.
70. J. Björklund, T. Miki, M. Andersson, and P.G. Jönsson: *ISIJ Int*., 2008, vol. 48 (4), pp. 438–45.